Energy Conversion and Management 354 (2026) 121152

Contents lists available at ScienceDirect

Energy Conversion and Management

journal homepage: www.elsevier.com/locate/enconman

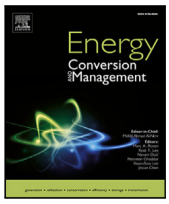

Research paper

# Evaluating the thermodynamic performance of an SOFC and PEMFC combined system

N.G.H. Goselink *, B.J. Boersma, L. van Biert

*Delft University of Technology, Maritime and Transport Technology, Mekelweg 2, Delft, 2628CD, Netherlands*

ARTICLE INFO

*Keywords:*
SOFC
PEMFC
Combined system
Thermodynamic analysis
Exergy analysis

ABSTRACT

This study investigates the integration of solid oxide fuel cells (SOFC) with proton exchange membrane fuel cells (PEMFC) to improve the system efficiency and minimise exergy losses from unused hydrogen. The paper offers new insights into the efficiency-power density trade-off of SOFC+PEMFC combined systems by simultaneously evaluating the systems' efficiency trends and their overall volume and mass. The SOFC+PEMFC is thermodynamically analysed and compared for the first time against an SOFC stand-alone system with anode off-gas recirculation (AOGR), another approach to increase efficiency by maximising the direct conversion of fuel into power. Simulations are run to reveal the impact of varying stack operating parameters, fuel utilisation, cell voltage, and operating temperature on the system efficiency, shape of the system's operational envelope, and overall volume and mass. An exergy analysis identifies major loss sources in the system and proposes pathways for improvement. The results demonstrate that integrating an SOFC with a PEMFC increases system efficiency to 55%, comparable to AOGR, while reducing the total system volume and mass by 20% and 23%, respectively. This study provides new insights into the potential use of SOFCs in volume and mass-limited applications such as long-distance transportation to reduce pollutant emissions.

## 1. Introduction

Global greenhouse gas (GHG) emissions continue to rise, while they should be falling to meet the goals in the Paris agreement [1]. In 2020, global GHG emissions totalled 47.06 billion tonnes, measured in carbon dioxide equivalents ($CO_2$eq), with electricity and heat production accounting for 32.2% of these emissions, followed by the transportation sector (including shipping and aviation) at 17.5% [2]. To break this trend, there is a strong push to look for cleaner alternatives. Solid oxide fuel cells (SOFC) represent a promising alternative to conventional energy conversion technologies due to their high conversion efficiencies (50%–60%), as opposed to aero-derivative gas turbines (GT) and reciprocating piston engines (RE) (25%–45%) [3,4]. High efficiency reduces fuel consumption, which results in reduced carbon emissions, while direct conversion of chemical energy into electrical energy largely prohibits the formation of $SO_x$, $NO_x$ and PM pollutants [5]. The high operating temperature allows the SOFC to be directly fed with different fuels such as natural gas, methanol and ammonia. Due to these advantages, the SOFC is interesting for long-distance transportation such as shipping [6] and aviation [7]. However, the limited gravimetric and volumetric power density of the SOFC, as well as their high cost, prevent it from being applied on a large scale.

Not all fuel delivered to the SOFC stack is consumed to prevent fuel starvation at the anode and associated cell damage [8,9]. The ratio of fuel used for the electrochemical reaction in the stack to the fuel delivered to the stack is the electrochemical fuel utilisation ($u_f$). Typically, the SOFC operates on a stack fuel utilisation of 60%–85%. In a stand-alone configuration, the unreacted fuel is mixed with the cathode off-gas and completely oxidised in an off-gas burner. Since simply burning the unreacted fuel represents a major exergy loss, the SOFC is sometimes combined with a thermal bottoming cycle that recovers the energy within the hot gasses leaving the SOFC system to optimize the electrical efficiency [10,11]. Different thermal bottoming cycles are investigated in the literature; gas turbines [12–14], reciprocating piston engines [5,15,16], Rankine cycles (RC) [17–19] and supercritical $CO_2$ cycles [20–22]. Although these systems promise significantly increased electrical efficiencies up to 70% [12,16], such results have not yet been replicated in practice, with efficiencies peaking at 53% [23]. Moreover, direct coupling between these components becomes more challenging under dynamic and part-load conditions [23,24]. Rather than burning the hydrogen, thereby converting it first into thermal energy and then into electrical energy, another approach is to convert the unused hydrogen directly into electrical energy.

* Corresponding author.
*E-mail address:* n.g.h.goselink@tudelft.nl (N.G.H. Goselink).

https://doi.org/10.1016/j.enconman.2026.121152
Received 7 September 2025; Received in revised form 30 December 2025; Accepted 29 January 2026
Available online 20 February 2026

One solution is the recirculation of the anode off-gas (AOGR) to the inlet and mix it with the fresh fuel. This increases the amount of fuel consumed in the system and hence the efficiency [25]. Unfortunately, not all the unreacted fuel can be recirculated, as the carbon contained in the anode off-gas of hydrocarbon fuels could deposit onto the anode, degrading its performance. Thus, part of the fuel is still being burned.

Another approach that optimises the fuel use within the system is the combination with a proton exchange membrane fuel cell (PEMFC) that directly converts the chemical energy into electrical energy. Although this combination seems thermodynamically less favourable, since low-temperature PEMFC does not utilise the waste heat, its high electrochemical fuel utilisation and energy efficiency are expected to offset these drawbacks [26]. The electrochemical fuel utilisation of such a system is comparable to, or even higher than, that in AOGR systems. Moreover, because the gravimetric and volumetric power density of the PEMFC is much higher than that of the SOFC [27], this combination has the added benefit of potentially reducing the system's size and mass compared to stand-alone systems with and without AOGR. The absence of an off-gas-burner also eliminates any combustion-related emissions such as $NO_x$, PM, CO and $SO_x$ [28], while carbon capture becomes more cost-effective [29,30]. Other benefits of this system over stand-alone SOFC include a higher technological maturity level and improved transient behaviour. Given the PEMFC's low tolerance to impurities, the SOFC anode off-gas must be purified before it can be fed to the PEMFC. Different purification technologies are reported in the literature, such as pressure swing adsorption (PSA) [29], temperature swing adsorption (TSA) [31] and membrane separation [32]. Although integrating these technologies adds volume, mass and complexity as well as an increase in auxiliary power demand, the combined SOFC+PEMFC system is considered a promising solution to increase the system efficiency and power density beyond the limitations of existing SOFC stand-alone systems.

Recent studies have evaluated different SOFC+PEMFC combined system architectures. Tan et al. [33] studied an SOFC+PEMFC combined system operating on methane. The parametric study revealed a positive correlation between the steam-to-carbon ratio, operating pressure and temperature, and system efficiency, which reached up to 60%, reportedly outperforming SOFC stand-alone, Reformer-PEMFC and SOFC-GT systems. Using natural gas as fuel, Wu et al. [31] evaluated a similar type of system, including TSA for hydrogen purification. With the conversion efficiency peaking at 64%, it is suggested to outperform SOFC stand-alone, Reformer-PEMFC and SOFC+GT/RE systems. The reported system comparisons in both [31,33] were limited to a single-point energy efficiency analysis based on literature-derived data. Meng et al. [34] investigated a methanol-operated system, with a peak system efficiency of 57%. The authors evaluated different SOFC and PEMFC integration architectures and highlighted the impact of varying the SOFC and PEMFC cell voltage on the PEMFC power output. To overcome the issue of CO poisoning, the authors opted to apply TSA technology and in a follow-up paper, they transitioned to ammonia as a fuel, achieving 62.6% efficiency [35]. Cai et al. [32] further improved this concept by incorporating AOGR into the PEMFC and using a Pd-Ag membrane to purify the hydrogen flow, resulting in the highest reported efficiency of 67.2%. An overview of the various systems, along with their specifications and performance, is presented in Table 1. Reported efficiencies vary strongly in the range 50%–67%, depending on the fuel type, SOFC stack operating parameters such as cell voltage ($U_{cell}$), fuel utilisation ($u_f$) and stack temperature ($T_{stack}$), and hydrogen purification method used. Considering these differences, it is difficult to draw meaningful conclusions about the efficiency potential of SOFC+PEMFC systems, especially in comparison to SOFC stand-alone systems, which typically achieve efficiencies in the range 50 to 60%. Most studies focus on peak efficiency optimisation, often neglecting the effect on the power density. The latter is an important aspect in long-distance transportation applications, where the efficiency-power density trade-off should be considered. Moreover, the reported efficiency gains are almost always benchmarked against conventional stand-alone SOFC system efficiencies found in literature without considering the SOFC+AOGR system. According to Peters et al. such a system including AOGR, can reach conversion efficiencies up to 66% [25], making it a more relevant comparison to SOFC+PEMFC systems.

Based on the foregoing literature review, the authors identified three key research gaps.

First, no prior studies investigated the influence of combining the SOFC with PEMFC on the system's gravimetric and volumetric power density. An essential consideration for the use of SOFCs in volume and mass-limited applications such as long-distance shipping and aviation.

Second, there has been no comparative analysis between this system and SOFC+AOGR systems, another approach for maximising the direct chemical-to-electric energy conversion that can reach efficiencies competitive with SOFC+PEFMC.

Third, previous system evaluations have focused on varying stack operating parameters separately and limited the system comparison to a single-point energy efficiency analysis based on literature-reported data. For a comprehensive system comparison, the different systems should be modelled and simulated in-house, to control the different system assumptions and parameters used for the calculations. This work applies a multi-variable parameter analysis whereby stack operating parameters are simultaneously varied. Moreover, results are mapped within the system's operational envelope to identify unfeasible operating regimes and efficiency trends, which allows us to compare these systems based on their full operational envelope instead of a single design-point efficiency. An additional consideration is the choice of $H_2$ purification technology. Though this work opts to include PSA, a sensitivity analysis is conducted that evaluates the impact of this design choice on the system efficiency. By running the model with and without pressurisation, the impact of incorporating PSA is evaluated and its effect on the results and conclusions can be estimated.

The main contributions of this paper are summarised as:

1. This paper offers a new perspective on the efficiency-power density trade-off in SOFC+PEMFC combined systems by simultaneously evaluating the impact of adding the PEMFC on the efficiency trends and gravimetric/volumetric power density. These are key aspects for the application in long-distance transportation.
2. This study introduces a novel comparison between the SOFC+PEMFC and SOFC+AOGR systems, to better benchmark the SOFC+PEMFC performance potential. Both approaches aim to optimise the direct conversion of fuel into power to maximise efficiency and reduce losses from unused hydrogen.
3. This paper presents a more comprehensive and systematic comparison of the different systems by evaluating their full operational envelopes and both energy and exergy efficiency trends. Through in-house modelling and simulation of the different systems, a more thorough system comparison is made possible than would be with a single-point analysis based on literature-derived data.

Thermodynamic analysis is a common approach to analyse the performance of power systems in terms of energy and exergy efficiency. This approach has previously been applied to SOFC-based systems [37,38] and is also used to investigate various SOFC+PEMFC system configurations [29,31–36] The thermodynamic analysis presented in this paper compares the SOFC+PEMFC with an SOFC stand-alone reference system and an SOFC system with AOGR. These system architectures are modelled using the Cycle-Tempo flowsheet software. Simulations are run for a variation in stack operating parameters, cell voltage, fuel utilisation and stack temperature. The resulting system performance e.g. efficiency, is presented as mapped contours within the system's operating envelope. A further system comparison shows that

**Table 1**
Values of SOFC input parameters, e.g. cell voltage ($U_{cell}^{sofc}$), fuel utilisation ($u_f^{sofc}$) and stack temperature ($T_{stack}^{sofc}$) for SOFC+PEMFC systems reported in literature. Performance metrics are the total power delivered ($P_{el}$), the net electrical efficiency ($\eta_{net,el}$) and the ratio of power delivered by PEMFC ($f_{P,pemfc}$). (*WGS*, water-gas-shift; *PrOX*, preferential oxidation; *TSA*, thermal swing adsorption; *PSA*, pressure swing adsorption).

| Reference | $U_{cell}^{sofc}$ [V] | $u_f^{sofc}$ [–] | $T_{stack}^{sofc}$ [°C] | $\eta_{net,el}$ [%] | $P_{el}$ [kW] | $f_{P,pemfc}$ [–] | CO-removal | $H_2$ purification |
|---|---|---|---|---|---|---|---|---|
| Meng (2023) [35] | n/a | 0.50 | 800 | 62.6 | 1278 | 0.48 | n/a | n/a |
| Meng (2022) [34] | 0.65 | n/a | 800 | 57 | 350 | 0.71 | WGS | TSA |
| Wu (2018) [31] | 0.75 | 0.80 | 750 | 64 | 644 | 0.22 | WGS | TSA |
| Tan (2015) [33] | 0.91 | 0.60 | 800 | 60 | 207 | 0.17 | WGS+PrOX | n/a |
| Rabbani (2014) [36] | n/a | 0.80 | 715 | 57.4 | 10.8 | 0.07 | n/a | n/a |
| Kim (2023) [29] | 0.7 | 0.70 | 800 | 50.2 | 1486 | 0.11 | WGS+PrOX | PSA |
| Cai (2024) [32] | n/a | n/a | n/a | 67.2 | 2202 | 0.13 | n/a | Membrane |

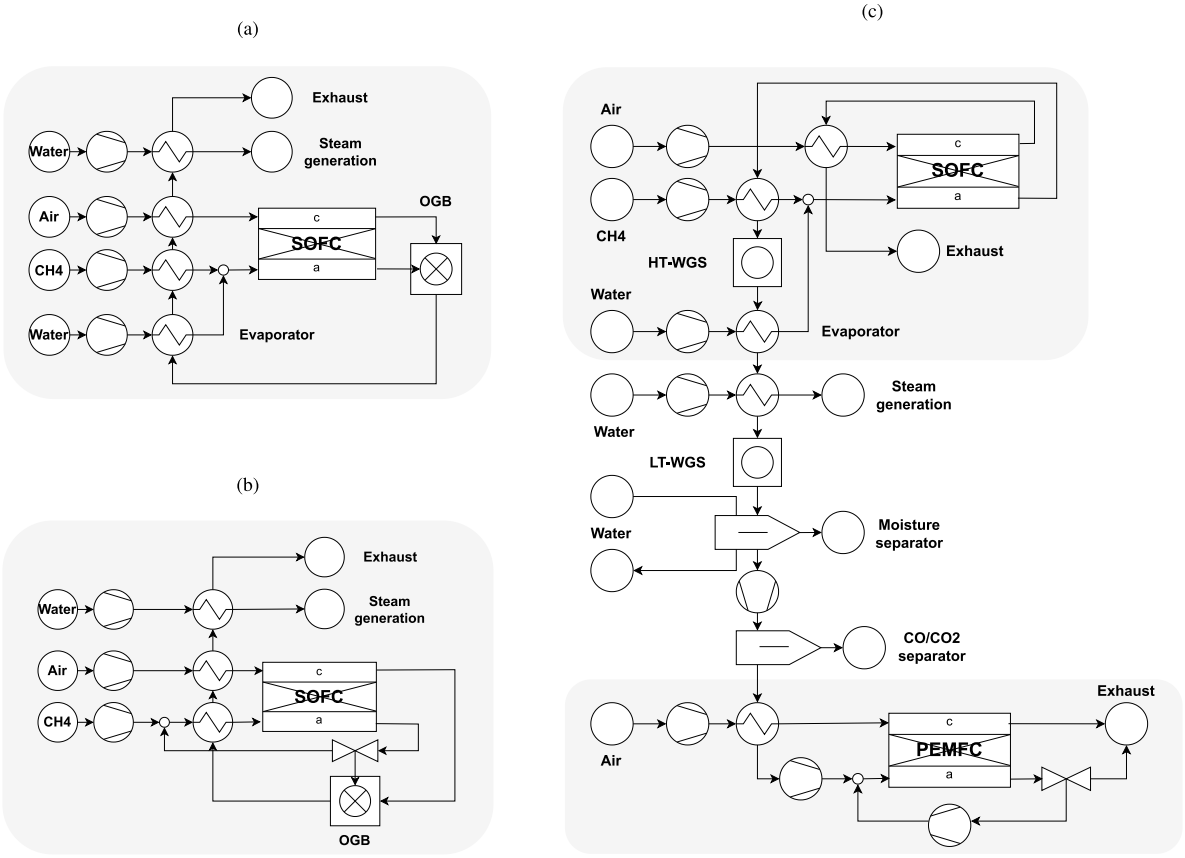


**Fig. 1.** Flowsheets of the investigated systems, stand-alone SOFC reference system (a), stand-alone SOFC system with AOGR (b) and SOFC+PEMFC combined cycle system (c). (*WGS*, water-gas-shift reactor; *OGB*, off-gas burner).

the SOFC+PEMFC system's size and mass can be reduced significantly, while increasing the electrical efficiency of the system compared to the stand-alone systems. The influence of using PSA hydrogen purification technology on the system efficiency decreases at higher fuel utilisation and cell voltage levels. These outcomes are particularly interesting for long-distance transport applications such as intercontinental shipping and aviation, where size, mass and cost are key performance characteristics.

## 2. SOFC system architectures

Flow sheets of the three systems investigated in this work are presented in Fig. 1. The first is a stand-alone SOFC reference system without AOGR (Fig. 1(a)), the second is a stand-alone SOFC system with AOGR (Fig. 1(b)) and the third is the SOFC+PEMFC combined cycle system (Fig. 1(c)).

All three systems are assumed to operate on methane ($CH_4$), which the SOFC internally converts into a hydrogen-rich gas through methane steam reforming (MSR) and the water-gas-shift (WGS) reactions:

$$CH_4 + H_2O \rightleftharpoons CO + 3\,H_2, \tag{1}$$

and

$$CO + H_2O \rightleftharpoons H_2 + CO_2. \tag{2}$$

MSR is used instead of other reforming methods such as catalytic partial oxidation and autothermal reforming, because it produces the most hydrogen and is more electrically efficient [39]. MSR is a strongly endothermic reaction that requires significant amounts of heat and steam, which it draws from the exothermic electrochemical reaction in the SOFC, the overall reaction is given in Eq. (3).

$$H_2 + \frac{1}{2}\,O_2 \longrightarrow H_2O \tag{3}$$

The reforming reaction occurs primarily at the entrance of the stack, whereas the electrochemical reaction accelerates towards the outlet [40]. These conditions favour solid carbon formation by methane

dissociation near the stack inlet, affecting the cell performance stability and resulting in a significant temperature gradient along the anode [40,41]. To prevent this, part of the methane is pre-reformed before entering the anode such that the $CH_4$ partial pressure is lowered, while heat and steam are provided in abundance at the anode inlet. This steam is provided either by evaporating an additional water stream with high-temperature anode off-gas, or by recirculating part of the steam-rich anode off-gas.

### 2.1. Stand-alone SOFC reference system

The stand-alone SOFC reference system without AOGR, hereinafter referred to as 'SOFC reference system', is based on an architecture reported by Riensche et al. [42]. The anode and cathode off-gas streams are mixed and combusted in the off-gas burner to generate heat. This heat is used to preheat the fresh fuel and air, evaporate water into steam and superheat the steam for the SMR reaction. Any remaining heat is recovered at the system outlet. The exhaust flow is cooled down to 190°C, resembling an auxiliary steam generation process.

### 2.2. Stand-alone SOFC system with AOGR

The stand-alone SOFC system with AOGR, defined as the 'SOFC+AOGR system', is based on [43]. AOGR supplies heat and steam to the anode inlet, by recirculating the anode off-gas and mixing it with the fresh fuel. This not only increases the system efficiency, but it also lowers the single-pass stack fuel utilisation as part of the unreacted hydrogen is fed back to the stack. The remaining anode off-gas is mixed with the cathode off-gas and burned in the off-gas-burner to preheat the fuel and air flows. The unused heat is afterward recovered through a waste heat recovery process, similar to the reference system.

### 2.3. SOFC+pemfc combined cycle system

*SOFC sub-system*

The SOFC+PEMFC combined cycle system, hereinafter referred to as 'SOFC+PEMFC system', is a modification of the stand-alone SOFC reference system, where the PEMFC replaces the combustor. The anode off-gas, containing the unreacted hydrogen is used as fuel for the PEMFC. Since CO produced during the methane steam reforming (see Eq. (1)) is still present in the anode off-gas, this is converted into $H_2$ and $CO_2$ in two consecutive WGS reactors (Eq. (2)). WGS is preferred over preferential oxidation (PrOX) for CO-removal, as it does not lower the hydrogen concentration due to oxidation. The system incorporates a high- and low-temperature WGS reactor, which takes advantage of higher reaction rates at high temperatures and higher $H_2$ yields at lower temperatures [44]. Since the WGS component assumes chemical equilibrium, small amounts of CO are still present in the gas at the exit of the low-temperature WGS reactor. A hydrogen purification step is required to lower the CO concentration to levels that are not poisonous to the PEMFC.

*Hydrogen purification sub-system*

Since methane is used as fuel, the only contaminants in the dehumidified hydrogen stream are CO and $CO_2$ at concentrations of 0.5% and 46.0% respectively. The hydrogen is separated from these components through PSA, a common method for separating hydrogen from flue gas [45,46]. Membrane and metal hydride separation are other techniques used to purify hydrogen. However, these suffer from high cost, low membrane lifetime, long cycle times and a limited capacity for the removal of CO [45]. In addition, the commercial availability of the PSA enables us to estimate its size and mass and thereby the complete SOFC+PEMFC system size and mass more accurately. Therefore, PSA is considered the most suitable option, achieving high $H_2$ purity in the range 99-99.999%, with a recovery rate of 70%–90% [45,47,48]. The disadvantage of using PSA is the increase in auxiliary power demand due to the addition of one more compressor. The electrical efficiency penalty at default operating conditions is 3.3%pt., for a pressure ratio $\Pi = 10$ [-] and hydrogen recovery efficiency of 85%. This value is estimated by running the model twice, with and without pressurisation to 10 bar, and comparing the resulting system efficiency.

*PEMFC sub-system*

The PEMFC sub-system is based on a simple design [49] with a water-cooled stack operating at 60°C. The air is compressed and preheated by residual heat in the PEMFC cathode off-gas stream before entering the cathode. The hydrogen-rich gas is cooled before compression to match the stack's operating temperature. Because the PEMFC single-pass fuel utilisation is less than unity, the unused hydrogen is recirculated and mixed with fresh gas at the anode inlet. Besides hydrogen, water vapour is also present in the recirculated flow, which helps in pre-humidifying the anode inlet. To achieve a relative humidity of 75% at the anode inlet, the recirculation ratio is fixed at 0.8.

## 3. Method

### 3.1. Cycle-tempo calculations

Cycle-Tempo, an in-house developed flow-sheet software, is used for the thermodynamic evaluation of the investigated systems. It contains a library of components such as chemical reactors, pumps, combustors, fuel cell stacks, etc., to model power plants. Each component adds mass and energy equations to a system matrix, that is solved iteratively to determine each component's pressure, mass flow, temperature and flow composition. The results are used to analyse the thermodynamic performance of different power plant architectures, for example, the system efficiency and exergy analysis [50]. This modelling software is commonly used in SOFC-based power plant research [11,37,38,51].

Cycle-Tempo employs a Gibbs free energy minimisation routine for equilibrium calculations in the combustor, reactor and fuel cell models. First, the inlet gas is taken to equilibrium in the fuel cell modules. The operating point of the SOFC is defined by specifying the power generation $P_{el,AC}$ and the cell voltage $V_{cell}$. The other parameters, such as current $I$ and power generated by the stack $P_{el,DC}$, are calculated from this input data. These processes are assumed to occur at constant internal pressure, gas composition and temperature. Equations used in Cycle-Tempo calculations are based on [50], unless specified otherwise.

The required fuel mass flow at the anode inlet $m_a^{in}$ is calculated from the total current $I$ and fuel utilisation $u_f$, according to [37]

$$m_a^{in} = \frac{I M_a}{2F(y_{H_2}^{in} + y_{CO}^{in} + 4_{CH_4}^{in})u_f} \tag{4}$$

where, $y_i^{in}$ is the anode gas concentrations at the inlet, $M_a$ the molar mass of the anode gas and $F$ is the Faraday constant. The oxygen mass flow from the cathode to the anode $m_{O_2,c\to a}$ is also calculated from the total current I,

$$m_{O_2,c\to a} = M_{O_2}\frac{I}{4F} \tag{5}$$

where $M_{O_2}$ is the oxygen molar mass. The cathode mass flow is determined from the energy balance over the fuel cell since the outlet temperature is known.

A simplified isothermal model is used for the fuel cell, the model calculates the local processes along the direction of the flow at constant temperature $T$. The cell is discretised in the flow direction such that internal profiles for the flow concentrations and current density are calculated, used to determine the local reversible voltage. The position of the local variables along the profiles is indicated by subscript $x$. The reversible, no loss, voltage $V_{rev,x}$ is calculated according to [37]:

$$V_{rev,x} = V_{rev}^0 + \frac{\bar{R}T}{2F}\ln\left\{\frac{p_{O_2,c}^{1/2} p_{H_2,a}}{p_{H_2O,a}} \times p_{cell}^{1/2}\right\} \tag{6}$$

with standard reversible voltage $V^0_{rev}$, universal gas constant $\bar{R}$, temperature $T$, mole fraction $y$ and partial pressures $p$ at standard state (1 bar). In reality, irreversibilities that occur within the cell will result in a cell voltage, $V_x$, smaller than the reversible voltage. This difference is indicated by the voltage loss $\Delta V_x$, the driving force of the electrochemical reaction. Voltage losses in the electrodes due to internal resistance are small compared to the losses in the electrochemical reaction or from transport losses in the electrolyte. This results in the assumption that the voltage is constant over the whole cell, $V = V_x$. The reversible voltage, however, does vary along the flow direction due to changes in temperature and reactant partial pressure. Therefore, as the voltage is constant, while the reversible voltage and voltage drop vary along the cell length, the following relation is obtained.

$$V = V_{rev,x} - \Delta V_x \tag{7}$$

For the voltage drop, the model assumes a linear correlation with the current density $i$ in the flow direction along the cell, shown in Eq. (8)

$$i_x = \frac{\Delta V_x}{R_{eq}}, \tag{8}$$

where $R_{eq}$ denotes the equivalent cell resistance. A detailed derivation of the cell resistance is given in [50]. The total current $I$ for the entire cell is eventually calculated according to:

$$I = \frac{u_f A}{R_{eq} \int_0^{u_f} d\lambda/(V_{rev}(\lambda) - V)} \tag{9}$$

where $A$ is the cell area and $\lambda$ is the dimensionless reaction coordinate. The cell power can be calculated using the known current and voltage.

For the PEMFC, the fuel mass flow is a given since it operates on the unreacted hydrogen of the SOFC. Because $H_2$ is the only reactant in a low-temperature fuel cell, the shift reaction does not occur in the stack. Eq. (4) is rewritten as:

$$I = \frac{m_{a,in}}{M_a} 2F y^0_{H_2} u_f. \tag{10}$$

The PEMFC is cooled using water, which is assumed to be under environmental conditions at the inlet of the pump (25°C, $p_{amb}$=1.103 bar).

### 3.2. System analysis

The main performance metric is the net electrical efficiency $\eta_{el}$ defined as:

$$\eta_{el} = \frac{P_{el,SOFC} + P_{el,PEMFC} - P_{aux}}{m_f LHV_{CH_4}}, \tag{11}$$

$P_{aux}$ is the total power consumption of all auxiliary components, such as pumps and compressors used in the SOFC, PEMFC and PSA subsystems. The efficiencies are calculated based on the lower heating value (LHV) of methane.

An additional metric of interest is the fraction of the total power delivered by the PEMFC, defined as:

$$f_{P,PEMFC} = \frac{P_{el,PEMFC}}{P_{el,PEMFC} + P_{el,SOFC}}, \tag{12}$$

which is an indication of the power split between SOFC and PEMFC power output. Based on this power split, the gravimetric and volumetric power density of the system can be calculated, using the values in Table 2. The PSA system size and mass are based on a commercially available system [48]. This system is linearly scaled such that the required feed flow matches the inlet flow into the PSA estimated by our model.

Exergy is the theoretical maximum amount of work that can be produced by bringing the system in equilibrium with its environment. Through an exergy analysis, which calculates the exergy of the various energy flows within the system, it is possible to identify the irreversibilities within each system component. Exergy analysis is a common method in thermodynamic engineering for determining not only where losses occur within a system, but also the magnitude of these losses. The relative exergy losses for each system are calculated at the nominal operating conditions (see Table 3). The environment definition used for the exergy calculation is the environment of Baehr ($p$ = 1 bar, $T$ = 25°C). The exergy loss per system component $k$ is calculated using an exergy flow balance:

$$\sum Ex_{loss,k} = \sum Ex_{in,k} - \sum Ex_{out,k}, \tag{13}$$

where the exergy of the process flow is the sum of physical, chemical, kinetic and potential exergy. Neglecting changes in kinetic and potential exergy, the exergy is calculated as:

$$Ex = Ex_{ph} + Ex_{ch}, \tag{14}$$

with $Ex_{ph}$ the physical exergy, and $Ex_{ch}$ the chemical exergy component. Physical exergy is the maximum useful work obtained from changes in a substance's physical state (temperature, pressure, and phase), defined as

$$Ex_{tm} = (H - H_0) - T_0(S - S_0), \tag{15}$$

where $S$ is the total entropy, $H$ the total enthalpy, and $T_0$ the environmental temperature. The subscript 0 refers to the enthalpy and entropy at the environmental state. Chemical exergy is the useful work potential related to chemical reactions in the process flow, defined as:

$$Ex_{ch} = \sum_{j=1}^{N} y_j \cdot ex_{j,0} + \bar{R}T_0 \sum_{j=1}^{N} y_j \cdot ln(y_j). \tag{16}$$

In Eq. (16), $\bar{R}$ is the universal gas constant, and $ex_j$ is the specific exergy of species $j$ at reference conditions indicated by the subscript 0. $y_j$ Is the molar fraction of the species that constitute the process flow; summing all $N$ species thus gives the flow's chemical exergy. To calculate the relative exergy loss for system component $k$, the exergy loss of that component is divided by the total absorbed exergy, the useful work potential, of the fuel.

$$Ex_{rel,k} = \frac{Ex_{loss,k}}{Ex_{f,absorbed}} \tag{17}$$

The stand-alone SOFC system models developed in *Cycle-Tempo* are validated with results from similar architectures reported in the literature. The SOFC reference system is validated against the results from [42], with only a 2% difference in electrical efficiency under similar operating conditions. Similarly, the SOFC+AOGR system shows good agreement with the results of [58], showing an offset in electrical efficiency of only 2%–3%.

### 3.3. SOFC anode recirculation

By recirculating part of the anode off-gas back to the anode inlet and mixing it with the fresh fuel, the amount of fuel consumed in the system changes. Therefore, a new parameter has to be introduced, the global fuel utilisation $u_{f,gl}$ defined as Eq. (20) in Table 4. It is a function of the single-pass fuel utilisation $u_{f,sp}$ and recirculation ratio $RR$. The combined effect of a variation in $RR$ and $u_{f,sp}$ on $u_{f,gl}$ is visualised in Fig. 2. First, the appropriate $RR$ is determined, which follows from [59]

$$RR = \frac{\dot{n}_{an,recycle}}{\dot{n}_{an,outlet}} = \frac{\text{O/C } ratio}{(2\text{C} + \text{H}/2 - \text{O})u_{f,gl}}, \tag{18}$$

where $C$, $H$ and $O$ are the number of carbon, hydrogen an oxygen atoms in the fuel molecule. The RR must be sufficiently high to supply abundant steam to the anode inlet and prevent solid carbon formation. An indicator for carbon formation in SOFCs is the oxygen-to-carbon (O/C) ratio, plotted for typical SOFC operating conditions in the inset in Fig. 2. Since carbon deposition is expected for O/C ratios ≤ 2, shown in grey in Fig. 2, the SOFC system in this work is operated at a constant O/C ratio of 2.25 (dashed line '- -'). Fig. 2 further shows that by increasing recirculation, the single-pass fuel utilisation can be

**Table 2**
Values for the gravimetric and volumetric power density of the SOFC, PEMFC and PSA systems.

| Parameter | Component | Range | Nominal value | Ref. |
|---|---|---|---|---|
| Gravimetric power density [W/kg] | SOFC | 8.8–22.44 | 20 | [52–54] |
| | PEMFC | 184.4–232.6 | 200 | [55–57] |
| System mass @feed flow capacity of 430 N $m^3$ [kg] | PSA | – | 2200 | [48] |
| Volumetric power density [W/l] | SOFC | 4.2–11.7 | 10 | [52–54] |
| | PEMFC | 98.1–103.88 | 100 | [55–57] |
| System volume @feed flow capacity of 430 N $m^3$ [l] | PSA | – | 7424 | [48] |

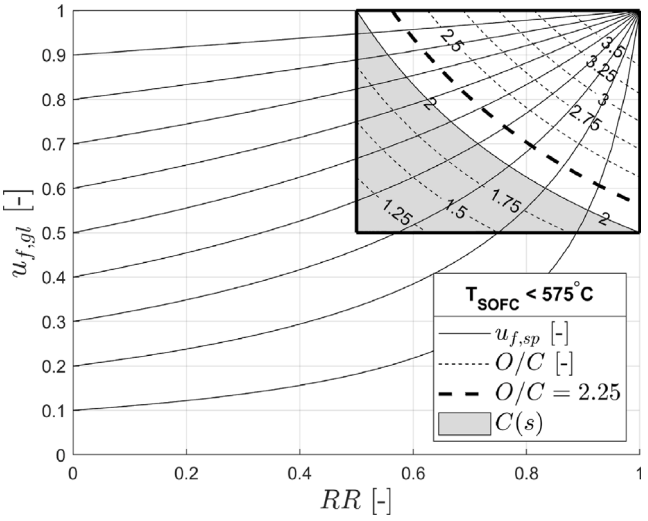


**Fig. 2.** Contours of single-pass fuel utilisation and O/C ratio for a variation in global fuel utilisation and anode recirculation ratio.

**Table 3**
Overview of the parameters varied in the analysis, with their respective range, interval and default values.

| Parameter | Range | Interval | Default value |
|---|---|---|---|
| $U_{cell}^{sofc}$ [V] | 0.6–0.9 | 0.025 | 0.7 |
| $u_{f,sp}^{sofc}$ [–] | 0.5–0.925 | 0.025 | 0.8 |
| $T_{stack}^{sofc}$ [°C] | 600–900 | 50 | 800 |

lowered while maintaining a specific global fuel utilisation. When no recirculation is applied, $RR = 0$, the system fuel utilisation equals the single pass fuel utilisation, as is the case for the reference SOFC system, Eq. (19) in Table 4.

### 3.4. Parametric analysis

All systems are subjected to a multi-variable parametric analysis of SOFC operating variables; two parameters are varied simultaneously to create a 2D grid of operating points. The efficiencies calculated for each system are then mapped onto this grid. The SOFC cell voltage ($U_{cell}^{SOFC}$) is varied from 0.6 to 0.9. The single-pass fuel utilisation ($u_{f,sp}^{SOFC}$) is varied from 0.5 to 0.925 and the stack operating temperature ($T_{stack}^{SOFC}$) is varied between 600°C and 900°C. Their respective ranges, typical operating ranges for SOFC, intervals and default values are also reported in Table 3. The PEMFC operating parameters are kept constant at the nominal values so as to focus solely on the influence of the SOFC on the rest of the system.

As mentioned in the previous section, the recirculation ratio is adjusted to maintain an $O/C_{ratio}$ of 2.25 for a variation in $u_{f,sp}^{SOFC}$, thereby increasing the system hydrogen consumption. Similarly, the addition of the PEMFC in the SOFC+PEMFC system also increases the electrochemical hydrogen consumption. The definition of the system fuel utilisations for the different SOFC architectures is given by Eqs. (19)–(21) in Table 4 and the resulting values are plotted at the top of the each graph in Figs. 3 and 4. The other input parameters, used for the simulations in this study, are given in Table 5.

**Table 4**
Definitions of system fuel utilisation ($u_{f,gl}^{sys}$) used for the system comparison.

| System type | Definition system fuel utilisation | Eq. |
|---|---|---|
| SOFC ref. system | $u_{f,gl}^{sys} = u_{f,sp}^{SOFC}$ | (19) |
| SOFC+AOGR system | $u_{f,gl}^{sys} = \frac{u_{f,sp}}{1-RR(1-u_{f,sp})}$ | (20) |
| SOFC+PEMFC system | $u_{f,gl}^{sys} = u_{f,sp}^{SOFC} + (1-u_{f,sp}^{SOFC}) \cdot \eta_{H_2,recov.} \cdot \frac{u_{f,sp}^{PEMFC}}{1-RR\cdot(1-u_{f,sp}^{PEMFC})}$ | (21) |

**Table 5**
Parameters used for the calculations. The reported values are based on values from [11,25,43].

| Parameter | Unit | Value |
|---|---|---|
| General | | |
| Heat exchanger pressure drop, $\Delta p$ | [bar] | 0.05 |
| Steam generation equipment pressure drop, $\Delta p$ | [bar] | 0.5 |
| Isentropic efficiency compressor, $\eta_{is}$ | [–] | 0.7 |
| Mechanical efficiency compressor, $\eta_{me}$ | [–] | 0.8 |
| DC-AC converter efficiency, $\eta_{conv}$ | [–] | 0.95 |
| HT-WHR outlet temperature, $T_{out}^{HT-WHR}$ | [°C] | 190 |
| LT-WHR outlet temperature, $T_{out}^{LT-WHR}$ | [°C] | 100 |
| SOFC | | |
| Stack inlet temperature, $T_{in}^{sofc}$ | [°C] | $T_{st}^{SOFC} - 50$ |
| Stack outlet temperature, $T_{out}^{sofc}$ | [°C] | $T_{st}^{SOFC} + 50$ |
| Anode pressure drop, $\Delta p_{an}$ | [bar] | 0.05 |
| Cathode pressure drop, $\Delta p_{ca}$ | [bar] | 0.05 |
| Power output, $P_{SOFC,AC}$ | [kW] | 1000 |
| Operating pressure, $p^{SOFC}$ | [bar] | 1.013 |
| Hydrogen cleaning & purification | | |
| HT-WGS reaction temperature, $T^{HT-WGS}$ | [°C] | 800 |
| LT-WGS reaction temperature, $T^{LT-WGS}$ | [°C] | 350 |
| Fraction of CO separated, $\chi_{CO}$ | [mole %] | 100 |
| Fraction of $CO_2$ separated, $\chi_{CO_2}$ | [mole %] | 99.5 |
| Hydrogen recovery percentage, $\eta_{H_2,recov.}$ | [%] | 0.85 |
| PEMFC | | |
| Cell voltage, $U_{cell}^{PEMFC}$ | [V] | 0.7 |
| Fuel utilisation, $u_{f,sp}^{PEMFC}$ | [–] | 0.85 |
| Average stack temperature, $T_{st}$ | [°C] | 60 |
| Anode pressure drop, $\Delta p_{an}$ | [bar] | 0.05 |
| Cathode pressure drop, $\Delta p_{ca}$ | [bar] | 0.1 |
| Operating pressure, $p^{PEMFC}$ | [bar] | 1.013 |
| Oxygen utilisation, $u_{ox}$ | [–] | 0.5 |
| Recirculation ratio, $RR^{PEMFC}$ | [–] | 0.80 |

## 4. Results

First, the effect of changing SOFC operating parameters on electrical efficiency is presented as contour plots in Section 4.1. Next, the system architectures are compared in terms of electrical efficiency, system size and weight, and exergy efficiency, in Section 4.2.

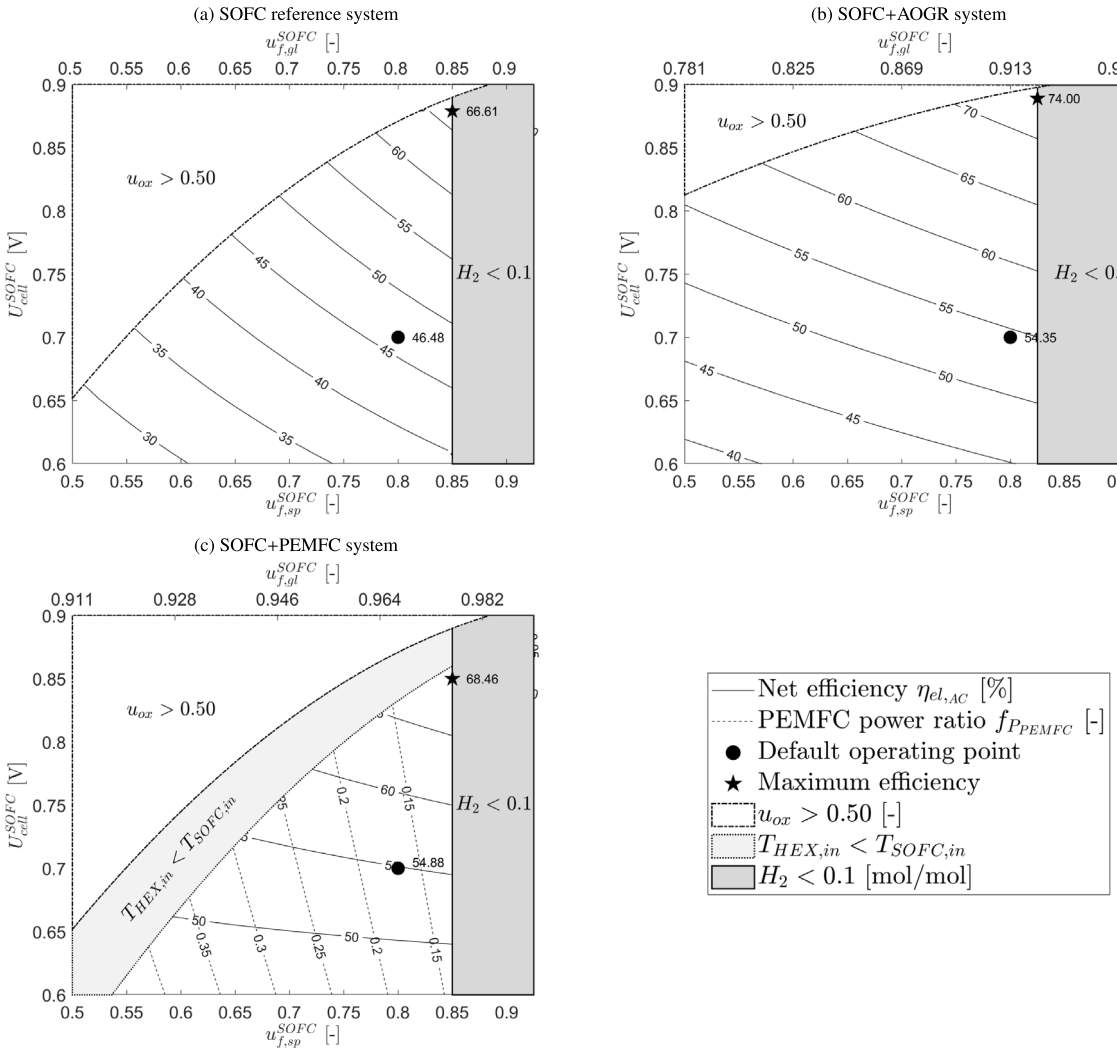


**Fig. 3.** Contour plots of net electrical efficiency ($\eta_{el,AC}$) for the SOFC reference system (Fig. 3(a)) and SOFC+AOGR system (Fig. 3(b)); and net electrical efficiency overlaid with fraction of total power delivered by the PEMFC ($f_{P,pemfc}$) for the SOFC+PEMFC system (Fig. 3(c)). Results are generated for a variation in SOFC fuel utilisation and cell voltage ($u_{f,sp}^{SOFC}$, $U_{cell}^{SOFC}$) under constant temperature ($T_{SOFC}$) and PEMFC operating conditions ($u_{f,sp}^{PEMFC}$, $U_{cell}^{PEMFC}$).

### 4.1. Varying SOFC operating parameters

For the SOFC parameter analysis, the results are categorised by operating parameters cell voltage and stack temperature. Contour plots are generated to show the combined effect of varying SOFC operating variables ($U_{cell}^{sofc}$ and $T_{stack}^{sofc}$ with $u_{f,sp}^{sofc}$).

#### 4.1.1. Cell voltage

Fig. 3(a) shows contours of net electrical efficiency for the SOFC reference system for a variation in SOFC single-pass fuel utilisation and cell voltage. Since less waste heat is produced at high cell voltages and lower fuel consumption levels, less cathode air is required to cool the stack and oxygen utilisation increases. Oxygen utilisation percentages higher than 50% ($u_{ox} > 0.50$) are to be avoided, as they increase cathode concentration losses [25]. Similarly, hydrogen concentrations at the anode outlet below 10% ($H_2 < 0.1$) risk fuel starvation and accelerated cell degradation [60], which is detrimental to the stack performance [8,9]. Since both these operating conditions are considered undesirable, they are omitted from Fig. 3(a). This results in a severely limited safe operating envelope, where the efficiency contours are only given for the feasible operating conditions. The net electrical efficiency increases for an increase in cell voltage and fuel utilisation since the electrochemical losses are reduced and less unused fuel leaves the stack. The electrical efficiency at the default operating point ($U_{cell}^{sofc}$ = 0.7 V and $u_{f,sp}^{sofc}$ = 0.80), marked by the black dot (•), is 46.5%, while the maximum efficiency can reach up to 66.6% for $U_{cell}^{sofc}$ = 0.875 V and $u_{f,sp}^{sofc}$ = 0.85, marked by the black star (⋆).

Fig. 3(b) shows contours of net electrical efficiency for the SOFC+AOGR system. Because part of the unreacted hydrogen is recirculated to the anode inlet, the amount of hydrogen used in the system increases. This system fuel utilisation ($u_{f,gl}^{sofc}$) is plotted at the top of the graph and reaches 0.923. The maximum efficiency that can be reached is 74.0%, while the efficiency at the default operating point (54.4%) is significantly higher than in the reference system. The mixing with recirculated hydrogen reduces the amount of fresh fuel required and thereby the cooling effect due to internal reforming. More cathode air is required to cool the stack, which reduces the oxygen utilisation and broadens the safe operating envelope. As a result, higher cell voltages can be achieved, which increase the system's peak efficiency potential. Since $CO_2$ is also recirculated, the hydrogen concentration at the stack outlet decreases slightly, reducing the safe operating envelope to $u_{f,sp}^{sofc}$ = 0.825.

Fig. 3(c) shows contours of constant electrical efficiency for the combined SOFC+PEMFC system overlaid with contours of the fraction of total power delivered by the PEMFC. Including the PEMFC increases the overall fuel utilisation up to 0.973. The oxygen and fuel utilisation

limits are similar to those of the reference system. Since the unused hydrogen is no longer combusted, the stored chemical energy is not released and less heat is available to pre-heat the fresh reactants and generate steam for steam-methane reforming. The operating points in this region, where $T_{HEX,in} < T_{SOFC,in}$, are therefore omitted from Fig. 3(c). The influence of SOFC fuel utilisation on the efficiency is small at lower cell voltages ($U_{cell}^{sofc} < 0.75$ V). The net electric efficiency increases marginally with an increase in $u_{f,sp}^{sofc}$ over the feasible operating envelope, which shows that the power balance can shift towards the PEMFC without significantly affecting the efficiency. The system fuel utilisation exceeds 0.91 regardless of the SOFC fuel utilisation, this is much higher than in case of AOGR. The electrical efficiency at the default operating point is 54.9%, a 8.4%pt. increase compared to the reference system, but only 0.5%pt. higher than the SOFC+AOGR system. The efficiency peaks at 68.5% for $U_{cell}^{sofc} = 0.85$ V and $u_{f,sp}^{sofc} = 0.85$, which is 1.9%pt. higher than the reference system. The maximum SOFC+PEMFC efficiency is 5.5% lower than the peak efficiency of the SOFC+AOGR system, due to the lower cell voltages that can be achieved. The PEMFC power output is inversely proportional to the SOFC fuel utilisation, as it depends on the hydrogen available at the SOFC anode outlet. The highest efficiency is achieved when the fraction of power delivered by the PEMFC is minimal, as the SOFC efficiency is higher than the PEMFC efficiency.

#### 4.1.2. Stack temperature

Fig. 4(a) shows that the contours of electrical efficiency are almost constant with stack temperature since a variation in temperature does not affect cell voltage in the current model. Oxygen utilisation levels over 50% only occur for $u_{f,gl}^{sys} < 0.55$ since the temperature required to cool the stack reduces. The efficiency at the default operating point is the same as in the previous set of contour plots. The maximum efficiency, 49.4%, is obtained at the maximum operating temperature of 900°C and a system fuel utilisation of 0.85. At this point, the least amount of unused fuel leaves the system, while the compressor's power demand is minimised.

Fig. 4(b) shows contours of electrical efficiency as a function of stack temperature for the SOFC+AOGR system. The efficiency trends display similar behaviour to the reference system. However, the region where $u_{ox} > 0.50$ is absent in this case since the amount of air required to cool the stack at each operating point is more than twice the amount of air required for the electrochemical reaction. The maximum efficiency increases to 56.8% at 900°C and $u_{f,sp}^{sofc} = 0.825$, the maximum fuel utilisation where there is still a sufficiently high hydrogen concentration at the anode outlet.

Fig. 4(c) shows results for the SOFC+PEMFC system. The region where $T_{HEX,in} < T_{SOFC,in}$ widens for operating temperatures over 800°C, as the reduction in airflow limits the enthalpy available to pre-heat the fresh reactants. The efficiency contour's level steps are smaller compared to the SOFC reference and SOFC+AOGR systems, indicating a smaller variation in efficiency over the entire operating envelope. The efficiency is observed to marginally increase with temperature due to the reduction in airflow and associated auxiliary power demand. The ratio of power produced by the PEMFC is independent of temperature and inversely proportional to fuel utilisation. Although the maximum efficiency of 55.5% is achieved at similar conditions to the reference system, it is almost 6% pt. higher than that of the reference system. Again, this is lower than that for the SOFC+AOGR system, but only 1.4% pt. in this case.

### 4.2. System comparison

To compare the different SOFC systems, another set of graphs is generated that displays trends in efficiency and the SOFC+PEMFC systems' normalised volume and mass for variations in fuel utilisation and cell voltage. The volume and mass of the SOFC+PEMFC system are normalised by dividing them by the volume and mass of the SOFC stand-alone system. In this case, the volume and mass of the SOFC reference and AOGR stand-alone systems are assumed to be the same.

Fig. 5(a) shows the normalised mass of the SOFC+PEMFC system overlaid with the net electrical efficiency of the different systems investigated for a variation in SOFC fuel utilisation within the SOFC+PEMFC's safe operating envelope. The SOFC+PEMFC system mass reduces with a decrease in fuel utilisation, as the power balance shifts towards the PEMFC, which has a higher power density. The exact percentages of mass reduction compared to the stand-alone systems are displayed at the top of the figure. The figure also shows a breakdown of the system mass into contributions by the SOFC, PSA and PEMFC subsystems. The SOFC remains the primary contributor across the entire range of $u_{f,gl}^{SOFC}$, while the PSA system is significanlty heavier than the PEMFC. The SOFC+PEMFC system's electrical efficiency is consistently higher than that of the other system investigated, across the entire range of fuel utilisations. This implies that the system mass can be significantly reduced by reducing the SOFC fuel utilisation, up to 23%, while maintaining an almost uniform electrical efficiency in the range of 53%–55%.

Fig. 5(b) shows the normalised system mass and system efficiency trends as a function of SOFC cell voltage. While varying the cell voltage, the SOFC fuel utilisation is kept constant at 0.8, at which point the weight reduction compared to the stand-alone systems is roughly 12%. Although the variation in system mass is small (<3%) for a variation in cell voltage, it is observed to reduce with a reduction in cell voltage. The reduction in stack efficiency requires more fuel to be fed to the SOFC, thereby increasing the hydrogen flow to the PEMFC. The trend in electrical efficiency of the SOFC+PEMFC is comparable to that of the SOFC+AOGR system. The values are almost equal, while both increase as a function of cell voltage at approximately an equal rate and are significantly higher than that of the reference system.

Figs. 5(c) and 5(d) show the influence of varying the SOFC fuel utilisation and cell voltage on the system volume. The general trends, in both normalised volume and efficiency, are the same as for the system mass in Figs. 5(a) and 5(b). Notable is the relative contribution of the PSA to the total volume, which is larger than in the case of the system mass. At the minimum fuel utilisation, the relative contribution by the PSA is nearly 8.8% of the total volume, while the relative contribution of the PEMFC is only 3.8%. A similar observation can be made for the variation in cell voltage, although at lower percentages (5.7% and 2.2% respectively). The percentages of volume reduction at the top of the figure further highlight that the addition of the PEMFC has a larger influence on the system mass than on the volume.

Integrating the SOFC with a PEMFC results in a system that is both more efficient and smaller in size and mass compared to the SOFC stand-alone systems, both with and without AOGR. Furthermore, reducing the system fuel utilisation is a significantly more effective approach in increasing the system's power density than lowering the cell voltage.

#### 4.2.1. Sensitivity analysis

The impact of incorporating PSA for hydrogen purification is assessed by simulating the model under pressurised and non-pressurised conditions, by adjusting the pressure ratio from 10 to 1. The latter represents the theoretical limit where the hydrogen purification process does not create back pressure in the system and pressurisation is not required. Other purification technologies, such as membrane or TSA, which require less parasitic power, will result in a system efficiency that is located within these boundaries. The hydrogen recovery efficiency is maintained constant at 85% during the simulations, recognising that even if pressurisation is not required, hydrogen losses still occur in the purification process. Fig. 6(a) plots electrical efficiency for both systems with and without pressurisation. The vertical lines visualise the difference in efficiency, the efficiency penalty, resulting from incorporating PSA. At lower SOFC fuel utilisations, the penalty is

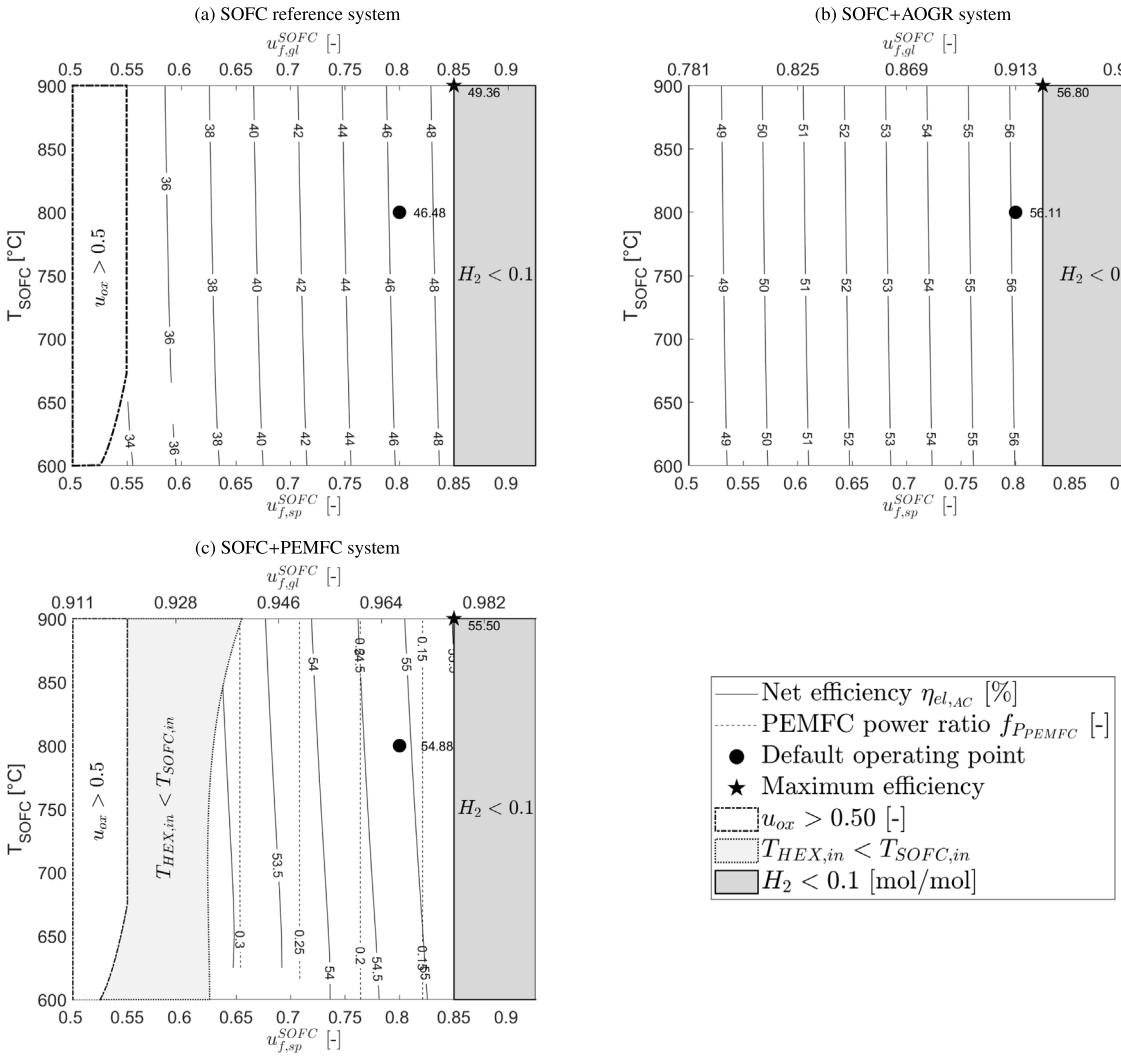


**Fig. 4.** Contour plots of net electrical efficiency ($\eta_{el,AC}$) for the SOFC reference system (Fig. 4(a)) and SOFC+AOGR system (Fig. 4(b)); and net electrical efficiency overlaid with fraction of total power delivered by the PEMFC ($f_{P,pemfc}$) for the SOFC+PEMFC system (Fig. 4(c)). Results are presented for a variation in SOFC fuel utilisation and stack temperature ($u_{f,sp}^{SOFC}$, $T_{SOFC}$) under constant cell voltage ($U_{cell}^{SOFC}$) and PEMFC operating conditions ($u_{f,sp}^{PEMFC}$, $U_{cell}^{PEMFC}$).

especially significant, as a high hydrogen flow results in large parasitic compression power. With an increase in fuel utilisation, the hydrogen concentration at the anode outlet reduces and the efficiency penalty decreases. Fig. 6(a) also shows the system efficiency to be even more uniform across the full range of fuel utilisations for the situation without pressurisation. Fig. 6(b) plots the compression power divided by the total parasitic power. At low fuel utilisation levels, the PSA power is by far the largest contributor to the total parasitic power demand. Given that the efficiency penalty reduces with a reduction in hydrogen flow to be pressurised, and that an increase in cell voltage lowers the hydrogen flow, it can be deduced that the peak efficiency of the SOFC+PEMFC system with PSA (68.5%) is only marginally lower than that of the system without PSA (69.3%) under high fuel utilisation and cell voltage conditions. Thus, the observations regarding peak efficiency will not change when purification processes are used that require less parasitic compressor power. Moreover, it also means that the difference at the default operating point is more significant, being 3.3%pt.

The sensitivity analysis also considered other operating parameters that were kept constant during the foregoing analysis, e.g., PEMFC cell voltage and fuel utilisation, and hydrogen recovery efficiency. Results are shown in Table 6. This table shows each parameter's nominal value, variation and percentage change in system electrical efficiency compared to the default efficiency according to Eq. (22).

$$\Delta\eta_{el} = \frac{\eta_{el} - \eta_{el,default}}{\eta_{el,default}} * 100\% \tag{22}$$

The default PEMFC fuel utilisation ($u_f^{PEMFC}$) and $H_2$ recovery efficiency ($\eta_{H_2,recov.}$) values are located towards the upper limit of their respective feasible ranges. An increase in both will not substantially increase the electrical efficiency. The largest efficiency gain is achieved by increasing the PEMFC cell voltage. Varying this parameter will increase the system efficiency with approximately 1–3%pt. Although this would result in a higher system efficiency, it will not change the main conclusions of this paper. The SOFC+PEMFC system efficiency is already higher than that of the other systems at the default SOFC operating ranges as seen in the graphs in Fig. 5, while the peak efficiency will not reach the value achieved by SOFC+AOGR.

### 4.2.2. Exergy analysis

The exergy losses for each system are calculated for a variation in SOFC fuel utilisation at the default cell voltage and temperature. A breakdown of losses per component as a function of fuel utilisation is presented in Figs. 7(a)–7(c). In addition, the exergy loss flows in *kW* and the relative exergy losses in % per component under default operating conditions are tabulated in Table A.7 in Appendix. To simplify the

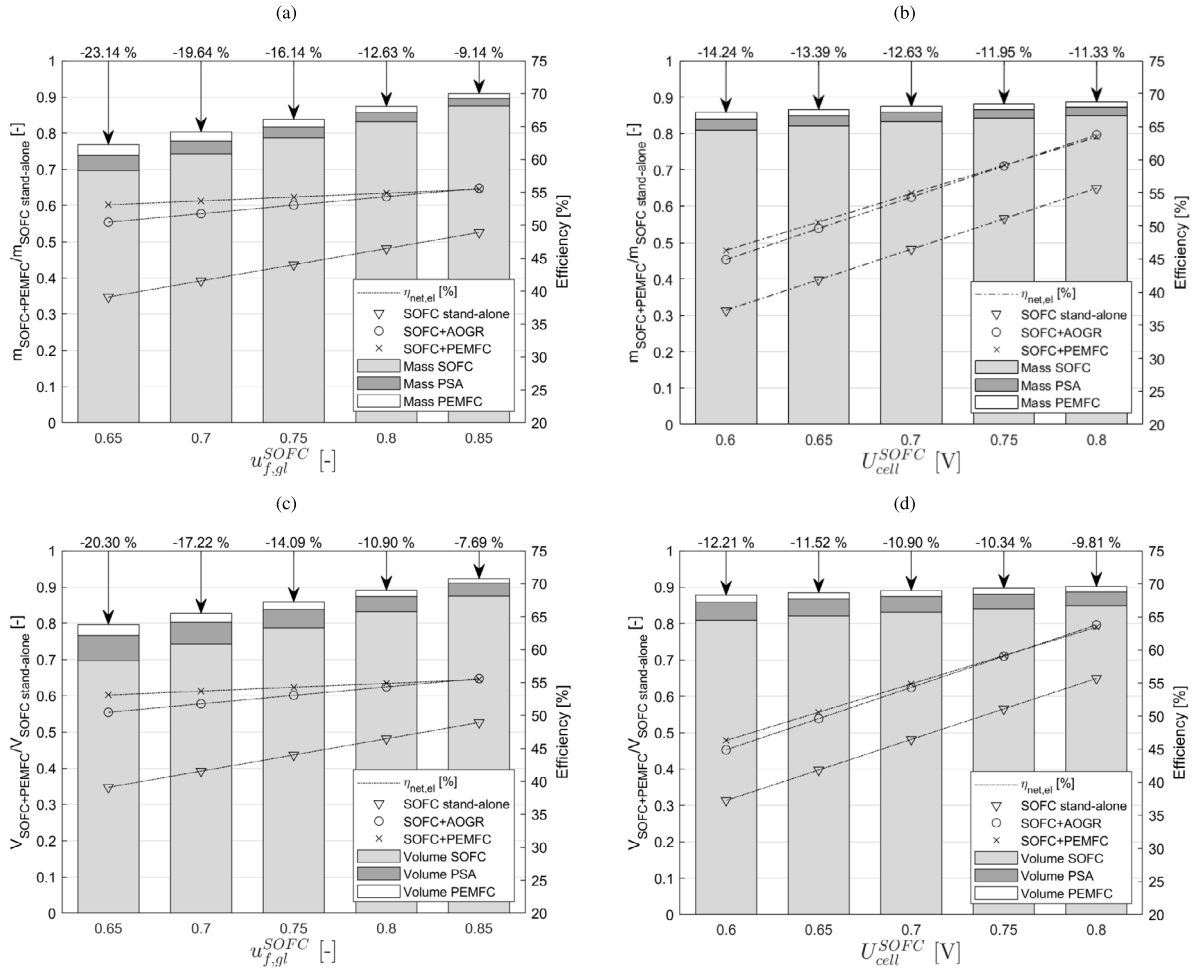


**Fig. 5.** Bar plots representing the SOFC+PEMFC systems' mass and volume normalised by the SOFC's stand-alone mass and volume overlayed with efficiency trends for the different systems investigated. Results are presented for a variation in fuel utilisation (Fig. 5(a) & 5(c)) and cell voltage (Fig. 5(b) & 5(d)). The fuel utilisation is varied for a constant cell voltage $U_{cell}^{SOFC}$ = 0.7 V and the voltage is varied for a constant fuel utilisation $u_f^{SOFC}$ = 0.8. The PEMFC operating conditions are kept constant at ($U_{cell}^{PEMFC}$ = 0.7 V, $u_f^{PEMFC}$ = 0.85).

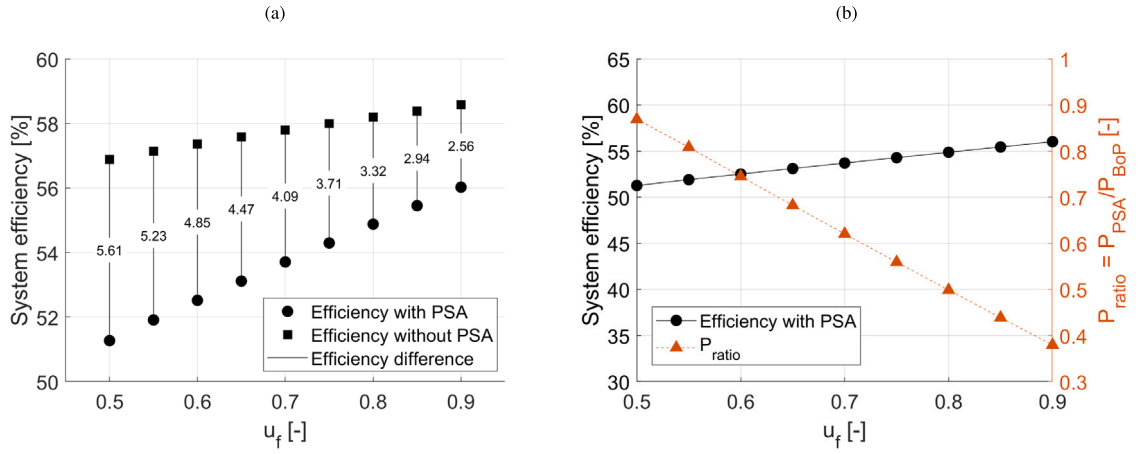


**Fig. 6.** Difference in electrical efficiency between systems with and without PSA by adjusting the pressurisation from 10 to 1 bar (Fig. 6(a)). Trends of system efficiency with PSA and ratio of pressurisation power $P_{PSA}$ over total balance of plant power $P_{BoP}$ (Fig. 6(b)). Data is gathered for a variation in SOFC fuel utilisation ($u_f^{SOFC}$) at a constant hydrogen recovery percentage of 85% and default operating conditions for the SOFC ($U_{cell}^{SOFC}$ = 0.7 V, $u_f^{SOFC}$ = 0.8) and PEMFC ($U_{cell}^{PEMFC}$ = 0.7, $u_f^{PEMFC}$ = 0.85).

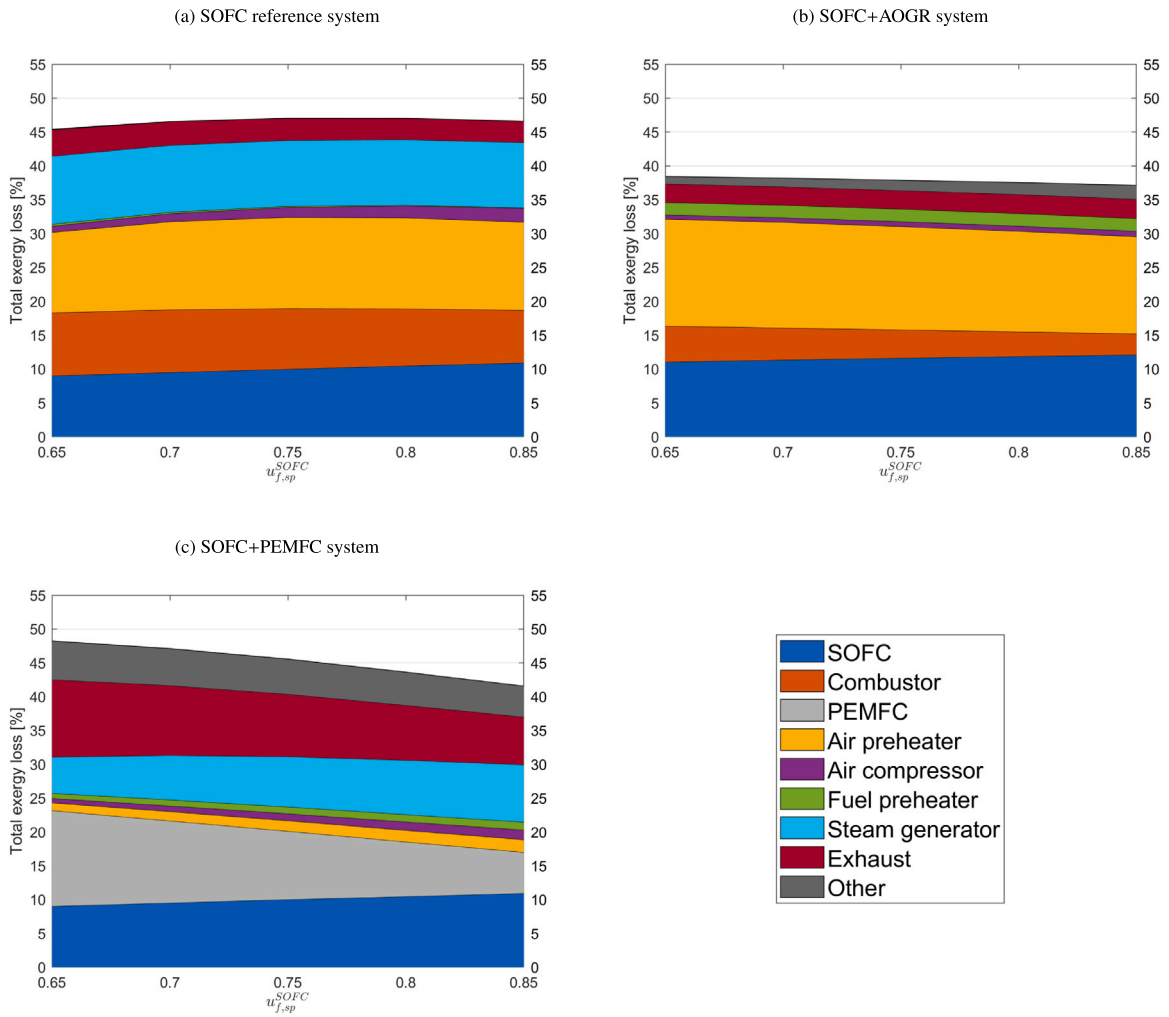


**Fig. 7.** Comparison of system's total exergy losses breakdown per component for the SOFC reference (Fig. 7(a)), SOFC+AOGR (Fig. 7(b)) and SOFC+PEMFC (Fig. 7(c)) systems for a variation in SOFC fuel utilisation at the default cell voltage ($U_{cell}^{SOFC}$ = 0.7 V) and SOFC operating temperature ($T_{SOFC}$ = 800°C). The PEMFC operating conditions are kept constant at ($U_{cell}^{PEMFC}$ = 0.7 V and $u_f^{PEMFC}$ = 0.85).

**Table 6**
Percentage change in net electrical efficiency compared to nominal values as a function of $u_f^{PEMFC}$, $U_{cell}^{PEMFC}$ and $\eta_{H_2,recov.}$. The electrical efficiency at nominal conditions is calculated for $u_f^{SOFC}$ = 0.8, $U_{cell}^{SOFC}$ = 0.7 V and $\Pi_{PSA}$ = 10. The system efficiency at default operating conditions, $\eta_{el,default}$ = 54.88%.

| Parameter | Nominal value | Set value | $\Delta\eta_{el}$ [%] |
|---|---|---|---|
| $u_f^{PEM}$ [–] | 0.85 | 0.5 | −2.57 |
| | | 0.6 | −1.62 |
| | | 0.7 | −0.87 |
| | | 0.8 | −0.27 |
| | | 0.9 | +0.23 |
| $U_{cell}^{PEM}$ [V] | 0.7 | 0.6 | −2.70 |
| | | 0.8 | +2.70 |
| | | 0.9 | +5.39 |
| $\eta_{H_2,recov.}$ [–] | 0.85 | 0.7 | −3.26 |
| | | 0.8 | −1.08 |
| | | 0.9 | +1.08 |

analysis, only major losses are considered in the breakdown analysis; all minor losses are accumulated under the term 'Other'.

Fig. 7(a) shows that the total exergy loss in the reference system is almost uniform with a variation in fuel utilisation. The majority of these losses can be attributed to four components: the SOFC stack (10.46%), combustor (8.44%), air preheater (13.44%) and steam generator (9.66%), compared to the total exergy loss of 47% at the default operating conditions. The dominant contributor is the heat transfer flow required to raise the cathode stream to the SOFC inlet temperature, which increases with fuel utilisation, as more cooling air is required. Exergy losses in the SOFC arise from electrical losses and chemical reactions, both of which increase steadily with fuel utilisation. The exergy destruction in the combustor stems from the combined effect of chemical reactions and (isothermal) mixing of the fuel and air. This loss reduces with an increase in fuel utilisation as the amount of hydrogen to be burned is smaller. Since the outlet temperature is reduced to 100°C by WHR, the exergy level in the exhaust gas flow remains low and almost constant with fuel utilisation. Meanwhile, exergy losses in the steam generation process, which consists of a boiler, evaporator and super-heater, reduce slightly with fuel utilisation. These losses can be eliminated by applying AOGR.

Fig. 7(b) presents a breakdown of exergy losses in the SOFC+AOGR system. Total exergy loss is reduced, primarily because the loss incurred by the combustor is more than halved (3.64%), while losses in the steam generation equipment are completely eliminated by AOGR. The lower exergy level in the combustor results from a reduction in the unused hydrogen that is combusted. In contrast, the exergy losses in the air pre-heater are higher than in the reference system (14.85%). Recirculation reduces the amount of fresh fuel required and thereby the amount of internal cooling. The increased air flow required for stack

cooling directly translates into an increase in heat transfer and associated exergy destruction. Simultaneously, as the SOFC fuel utilisation rises, the recirculation ratio decreases, allowing more fresh fuel to enter the system. This reduces the cooling demand again and subsequently lowers the air flow and associated exergy losses through the air preheater. Since the air preheater presents the largest exergy loss in the system, one possible strategy to lower this is to reduce the temperature gradient over the heat exchanger, thereby reducing irreversibilities. The waste heat recovery process is identical to the SOFC stand-alone systems, resulting in similar exergy levels at the exhaust.

A breakdown of the exergy losses in the SOFC+PEMFC system are shown in Fig. 7(c). As the SOFC fuel utilisation increases, the total exergy loss in the system reduces significantly from 48% at the lower fuel utilisation limit to 41.56% at the higher end. The majority of the losses occur in the SOFC (10.45%), PEMFC (8.08%), exhaust flow (8.13%) and steam generation equipment (8.02%). The combined fuel cell losses reduce with an increase in SOFC fuel utilisation. The relatively higher losses in the PEMFC, compared to the SOFC, result from the high amount of fuel utilisation in the PEMFC at lower $u_{f,sp}^{SOFC}$ conditions. Air preheater losses (1.72%) are drastically lower than those in the SOFC reference and SOFC+AOGR systems, due to the absence of a combustor. This limits the maximum temperature in the system to the SOFC outlet temperature, decreasing the temperature gradient across the heat exchanger and associated exergy losses. Additional exergy losses arise from the use of the PSA for hydrogen purification. These losses are most prominent in the compressor itself and in the high-temperature PSA-separated flow. The exergy loss at the PSA outlet results from the combined effect of the high flow temperature due to pressurisation and the discharge of unrecovered $H_2$ and $CO_2$ into the environment. Moreover, because waste heat recovery is applied before the hydrogen purification section, the temperature and exergy levels of the exhaust downstream are higher compared to the SOFC reference and SOFC+AOGR systems. This, along with the $H_2$ discharge, explains the increased contribution of exhaust-related exergy losses. Losses attributed to the hydrogen separation and purification equipment (water-gas-shift reactors, PSA and condenser) are grouped under 'other' losses.

Based on the identified loss sources, potential pathways to reduce the magnitude of these losses are proposed. As mentioned, the application of PSA for hydrogen purification introduced additional losses in the system. These include the compression and expansion of the flow to be purified, which account for 2.9% relative losses, and the discharge of unrecovered $H_2$ from the purification process, also accounting for 2.9%. This suggests that further optimisation of the hydrogen purification, e.g. lowering the pressure requirement, and increasing the $H_2$ recovery rate in the separation process, can significantly increase the exergetic efficiency of the system. An additional minor exergy saving of up to 0.5% can be made by applying WHR to the outlet of the purifier, lowering the flow's temperature from 340°C to 100°C. Besides hydrogen purification, steam generation is another major source of loss, accounting for 8.02% of the exergy losses at nominal conditions. The current steam generation system consists of three distinct heat exchangers: an economiser, an evaporator, and a superheater. Replacing these with a single flash heater reduces losses by 1.2%. However, a large heat transfer loss still remains. Alternatively, steam generation could be eliminated by partially incorporating AOGR, recirculating just enough anode off-gas to meet the steam demand for methane reforming. Although it could improve efficiency, this would come at the expense of system volume and mass. Finally, exergy losses in the SOFC and PEMFC themselves are harder to abate as losses related to chemical reactions and electrical conversion are inherent to fuel cell operation. Optimising operating conditions, such as temperature, pressure, and flow, could reduce exergy losses within the fuel cell. Examples include recirculating the cathode off-gas, which lowers the air preheating requirement, and increasing the operating pressure or temperature of the fuel cell. This increases the Nernst voltage and reduces irreversibilities within the cells, while also offering the potential for additional power generation downstream [50].

## 5. Discussion

A disadvantage of the SOFC stand-alone reference system is its inability to operate at system fuel utilisations exceeding 0.85, due to the $H_2$ concentration at the anode outlet dropping below 10 mol%. Incorporating AOGR or adding a PEMFC allows the electrochemical fuel utilisation of the system to increase beyond this point, positively affecting the system efficiency. Although the SOFC+AOGR system achieves the highest peak efficiency due to its ability to operate at higher cell voltages, the SOFC+PEMFC system is more efficient at lower cell voltages and fuel utilisation levels. In addition to its efficiency at these operating conditions, the SOFC+PEMFC system also benefits from a significant reduction in size and mass.

These presented outcomes are specific to the use of methane. Varying the fuel type might lead to different conclusions. Since a DIR-SOFC system assumes internal reforming of methane, a strongly endothermic reaction, the use of any other fuel will influence the internal cooling capacity. This affects the amount of cooling air required and, as a consequence, the operational envelope and electrical efficiency trends. The use of methanol is reported in [34] while the use of ammonia is reported in [32,35]. Similar to methane, methanol is a hydrocarbon fuel with the same carbon-to-hydrogen ratio, requiring similar levels of hydrogen purification. The example of ammonia shows that using this fuel could potentially increase the electrical efficiency, as ammonia-fuelled systems do not require CO removal and purification processes. These systems are also presented in Table 1, in which the ammonia-fuelled system shows the highest reported efficiency.

The SOFC+PEMFC's peak electrical efficiency is 69.80%, exceeding all reported values in Table 1. However, because these values vary strongly with SOFC operating conditions and hydrogen purification method, comparing them with similar systems from literature is difficult. The system architecture by Kim et al. [29] is most similar to our layout as it also operates on methane and includes PSA. The reported electrical efficiency reaches 50.2% for $U_{cell}$ = 0.7 V, $u_f^{sofc}$ = 0.70 and $T_{stack}$ = 800°C. This is lower than the 53.81% achieved in this work under identical conditions. This difference is most likely explained by the carbon capture in the system by Kim et al. which increases the system's auxiliary power demand. Wu et al. reported a peak efficiency of 64%, almost 5%pt. higher than our system achieves under similar SOFC and PEMFC operating conditions and also operating on methane. An obvious difference is the type of hydrogen purification technology. Wu et al. incorporated TSA in their system architecture, which reduces the auxiliary power demand. The foregoing sensitivity analysis revealed that excluding the PSA would result in an approximate efficiency increase of 3%pt., decreasing the difference to 2%pt. This difference falls within the expected uncertainty range attributed to assumptions regarding turbo-machinery efficiency and component pressure losses within the system. Therefore, based on this comparison, the authors believe that the modelled system is considered sufficiently validated.

Including pressure swing adsorption (PSA) for purification incurred an electrical efficiency penalty of approximately 3.3%pt. at default operating conditions. Without it, the peak efficiency of the SOFC+PEMFC would have been closer to the SOFC+AOGR system. The PSA also contributes to increased exergy losses, which can be attributed to two main loss sources. First, the PSA-separated flow, which is composed of CO, $CO_2$ and the $H_2$ that could not be recovered in the purification process. Releasing this $H_2$ into the environment represents a direct exergy loss. Increasing the hydrogen recovery percentage can reduce this loss. In the ideal case with no hydrogen loss, the exergy loss could be nearly halved. However, increasing the hydrogen flow to the PEMFC increases losses within this component, offsetting the efficiency gains and resulting in a net loss reduction of 1.8% pt. Second, the pressurisation process itself generates around 2.9%pt. of relative exergy loss. These losses originate in the compressor and are evident in the exhaust flow. Since pressurisation increases the flow temperature, the lack of heat recovery downstream results in an exergy loss. Replacing

the PSA with a membrane-based purification system improves the exergy efficiency by 4.5%pt., representing a significant efficiency gain. Alternatively, eliminating the hydrogen purification process completely is another option. The SOFC could be combined with an HT-PEMFC, which is characterised by a higher carbon monoxide tolerance. Another approach is connecting two SOFCs in series, as presented by Nehter et al. [61]. This setup achieved an electrical efficiency of 60%, roughly 5%pt. higher than currently achieved under similar conditions. The disadvantage of both these configurations is the lower power density of the HT-PEMFC and SOFC systems compared to the LT-PEMFC. This would significantly increase the system size and mass compared to the current architecture.

A thermodynamic analysis of different SOFC combined cycle systems (ambient SOFC-GT, pressurised SOFC-GT, SOFC-RC and SOFC-RE) are presented by van Biert et al. [11]. The peak electrical efficiencies achieved vary in the range of 66%–68%, which is in line with the peak efficiency achieved by the SOFC+PEMFC system (~68%). The net electrical efficiency across the SOFC+PEMFC's operating envelope varies from ~45 to 68%, which is similar to these combined cycle systems that achieve ~48%–68%. Our SOFC+PEMFC system can thus be considered competitive with these combined cycle systems in terms of electrical efficiency.

Using the SOFC as a pre-reformer to the PEMFC, allowing the PEMFC to operate on hydrocarbon fuels, seems not feasible due to the inability to sustain operation at low SOFC fuel utilisations. If the PEMFC is assumed to be the main power source, the SOFC fuel utilisation is required to drop below 0.5, resulting in oxygen utilisation ratios of over 50%, which is discouraged to prevent excessive degradation of the cells.

The current modelling and analysis are limited to steady-state conditions. Especially in transportation applications, the dynamic behaviour of such a system is an important aspect to consider. Including the PEMFC improves the system's dynamic response due to the PEMFC's superior dynamic characteristics. By shifting the power generation ratio towards the PEMFC, which can be achieved by operating the SOFC at a lower fuel utilisation, the system's dynamic performance can be further enhanced. This shift results in only a small efficiency trade-off, while it also benefits the system's size and mass. Moreover, adding a hydrogen tank between the SOFC and PEMFC, acting as an energy buffer, can help in operating the PEMFC more dynamically independent of the SOFC. The optimal power split between SOFC and PEMFC and sizing of both these components will depend on the specific application, such as the type of ship and its characteristic operational profile.

### 5.1. Future work

Different directions for future research have already been suggested in the foregoing discussion. The most promising topics are summarised in this paragraph.

Considering the growing interest in alternative fuels such as methanol, ammonia and hydrogen in the transportation sector and more specifically for maritime applications, it would be valuable to extend the analysis by including those fuels. As previously mentioned, varying the type of fuel will influence the system efficiency and operational envelope and may result in increased performance compared to methane-fuelled systems.

The present analysis is limited to steady-state conditions. A future study should include dynamic modelling to better understand the dynamic response of the SOFC+PEMFC system and compare its performance to stand-alone SOFC systems. A dynamic analysis is useful to accurately size the SOFC, PEMFC and possibly the hydrogen tank, which could function as an energy buffer in the system. This would further strengthen its case as a potential technology for use in long-distance transportation applications.

Lastly, this work focuses on the thermodynamic performance of the SOFC+PEMFC system in terms of energy and exergy efficiency, identification of feasible operating regimes and implications on the system size and mass, and not on the economic aspect. A techno-economic evaluation is outside the scope of the current work and is recommended for future research, especially since cost considerations are an important aspect for potential users of such a system. The technical analysis presented in this paper can serve as a foundation for such a future techno-economic analysis.

## 6. Conclusions

This study presented a thermodynamic analysis of the SOFC+PEMFC combined system. Results have been compared to SOFC stand-alone systems with and without anode off-gas recirculation (AOGR). The effect of varying fuel utilisation, cell voltage and stack temperature was assessed through a multi-variable parameter analysis. Results were presented as contour plots of constant efficiency and fraction of power delivered by the PEMFC within the system's operating envelope and as a comparative analysis of the system's overall size and mass

Operational limits such as fuel and oxygen starvation, as well as the enthalpy levels at the stack outlet for the SOFC+PEMFC system, severely limited the SOFC's safe operating envelope. Including a PEMFC increased the electrical efficiency at the default operating point ($U_{cell}^{SOFC}$ = 0.7 V, $u_{f,sp}^{SOFC}$ = 0.80 and $T_{stack}^{SOFC}$ = 800°C) to 54.9% and the maximum efficiency to 68.5% compared to the reference systems' default and peak efficiency of 46.5% and 66.6%, respectively. Although the SOFC+PEMFC system could not match the SOFC+AOGR peak efficiency (74%), it demonstrates superior efficiency at lower SOFC fuel utilisation ratios and cell voltages. Moreover, the nearly uniform electrical efficiency, with SOFC fuel utilisation at the default cell voltage, allows the power balance within the system to shift towards the PEMFC, without significantly affecting the efficiency. By doing so, large reductions in system size and mass are achieved. The system's overall system volume is reduced by as much as 20% and the system's mass decreased by up to 23%.

The impact of using pressure swing adsorption (PSA) for hydrogen purification has been evaluated through a sensitivity analysis. Results indicated an electrical efficiency penalty of 3.3%pt. at default operating conditions. However, the severity of this penalty reduces at higher fuel utilisation and cell voltage levels, to less than 1%pt. at the peak efficiency. In contrast, at the lower end of the feasible fuel utilisation range, electrical efficiency can be increased by 4–5%pt. when a hydrogen purification technology is applied that demands less electrical power.

An exergy analysis showed that the losses in the SOFC-PEMFC exceeded the reference system levels at lower fuel utilisation ratios. These losses decreased with an increase in fuel utilisation, yet it never outperformed the SOFC+AOGR system in terms of exergy efficiency. Exergy losses related to heat transfer were significantly reduced as the maximum temperature in the SOFC+PEMFC system was limited to the stack outlet temperature in the absence of an off-gas burner. The remaining exergy losses primarily originate from both fuel cells, the external steam generation required for reforming, and the hydrogen purification via PSA. Therefore, the greatest potential for further exergy loss reduction lies in optimising the hydrogen purification process, specifically, reducing compression losses and minimising the discharge of unrecoverable hydrogen, as well as optimising the steam supply to the anode inlet.

Integrating the SOFC with a PEMFC thus results in a system that can be both more efficient and smaller in size and mass compared to the SOFC reference and SOFC+AOGR systems. Including PSA does not notably affect the peak efficiency of the SOFC+PEMFC system, but has a more prominent effect on the electrical efficiency at lower $u_f^{SOFC}$. Optimising the hydrogen purification process can further increase the electrical and exergy efficiency in the range where the largest mass and volume reduction is achieved compared to the reference SOFC and SOFC+AOGR systems. Since system size and weight are crucial factors in adopting SOFCs in long-distance transportation, the SOFC+PEMFC system offers a potential path for applying SOFCs in intercontinental shipping and aviation to reduce greenhouse gas emissions.

**Table A.7**
Exergy comparison between the SOFC stand-alone, SOFC+AOGR, and SOFC+PEMFC systems. Data is generated at default fuel cell operating conditions ($u_f^{SOFC} = 0.8$, $U_{cell}^{SOFC} = 0.7$ V, $T_{stack}^{SOFC} = 800$°C, $u_f^{PEMFC} = 0.85$ and $U_{cell}^{PEMFC} = 0.7$ V).

| Component | SOFC stand-alone | | SOFC+AOGR | | SOFC+PEMFC | |
|---|---|---|---|---|---|---|
| | Exergy loss [kW] | Rel. Ex. loss [%] | Exergy loss [kW] | Rel. Ex. loss [%] | Exergy loss [kW] | Rel. Ex. loss [%] |
| SOFC | 212.86 | 10.46 | 198.52 | 11.87 | 213.19 | 10.45 |
| Combustor | 171.41 | 8.44 | 69.4 | 3.64 | – | – |
| PEMFC | – | – | – | – | 164.22 | 8.08 |
| Air preheater | 273.13 | 13.44 | 282.02 | 14.85 | 31.82 | 1.72 |
| Air compressor | 35.80 | 1.76 | 9.03 | 0.77 | 25.20 | 1.24 |
| Fuel preheater | 2.39 | 0.12 | 32.19 | 1.85 | 22.15 | 1.09 |
| Steam generator | 196.06 | 9.66 | – | – | 163.09 | 8.02 |
| Exhaust | 63.98 | 3.14 | 50.09 | 2.8 | 165.38 | 8.13 |
| Other | 0 | 0 | 36.57 | 1.76 | 102.51 | 4.9 |
| Total | 955.63 | 47.03 | 677.82 | 37.54 | 887.56 | 43.63 |

## CRediT authorship contribution statement

**N.G.H. Goselink:** Writing – review & editing, Writing – original draft, Methodology, Investigation, Formal analysis, Conceptualization. **B.J. Boersma:** Writing – review & editing, Supervision. **L. van Biert:** Writing – review & editing, Supervision, Methodology, Funding acquisition.

## Declaration of competing interest

The authors declare that they have no known competing financial interests or personal relationships that could have appeared to influence the work reported in this paper.

## Acknowledgements

This research is supported by the $SH_2$IPDRIVE project, which aims to accelerate the introduction of hydrogen as an alternative energy carrier in the Dutch maritime sector. The main goal is to develop reliable, safe, standardised and scalable solutions for zero-emission propulsion and energy systems on board ships. The project is funded by the Rijksdienst voor Ondernemend Nederland (RVO) under the R&D Mobiliteitssectoren regulation.

## Appendix. Exergy analysis

See Table A.7.

## Data availability

Data will be made available on request.

## References

[1] Paris agreement. Report, 2015, United Stations Treaty Collection, Chapter XXVII 7. d.
[2] Ritchie H, Rosado P, Roser M. CO2 and greenhouse gas emissions. Our World Data; 2023, https://ourworldindata.org/co2-and-greenhouse-gas-emissions.
[3] Wartsila. Combustion engine vs. Aeroderivative gas turbine - Executive summary. 2024, Web Page. 2024. URL: https://www.wartsila.com/energy/learn-more/technology-comparison-engines-vs-aeros/executive-summary.
[4] van Biert L, Godjevac M, Visser K, Aravind PV. A review of fuel cell systems for maritime applications. J Power Sources 2016;327:345–64. http://dx.doi.org/10.1016/j.jpowsour.2016.07.007.
[5] Yongming F, et al. Progress and prospect of the novel integrated SOFC-ICE hybrid power system: System design, mass and heat integration, system optimization and techno-economic analysis. Energy Convers Manag: X 2023;18. http://dx.doi.org/10.1016/j.ecmx.2023.100350.
[6] Baldi F, Moret S, Tammi K, Maréchal F. The role of solid oxide fuel cells in future ship energy systems. Energy 2020;194. http://dx.doi.org/10.1016/j.energy.2019.116811.
[7] Collins FM, McLarty D. All-electric commercial aviation with solid oxide fuel cell-gas turbine-battery hybrids. Appl Energy 2020;265. http://dx.doi.org/10.1016/j.apenergy.2020.114787.
[8] Fang Q, Blum L, Peters R, Peksen M, Batfalsky P, Stolten D. SOFC stack performance under high fuel utilization. Int J Hydrog Energy 2015;40(2):1128–36. http://dx.doi.org/10.1016/j.ijhydene.2014.11.094.
[9] Chen G, Guan G, Abliz S, Kasai Y, Abudula A. Rapid degradation mechanism of Ni-CGO anode in low concentrations of H2 at a high current density. Int J Hydrog Energy 2011;36(14):8461–7. http://dx.doi.org/10.1016/j.ijhydene.2011.04.046.
[10] Tronstad T, Hogmoen Astrand H, Haugom GP, Langfeldt L. Study on the use of fuel cells in shipping. Report, European Maritime Safety Agency; 2017.
[11] van Biert L, Woudstra T, Godjevac M, Visser K, Aravind PV. A thermodynamic comparison of solid oxide fuel cell-combined cycles. J Power Sources 2018;397:382–96. http://dx.doi.org/10.1016/j.jpowsour.2018.07.035.
[12] Cocco D, Tola V. Externally reformed solid oxide fuel cell–micro-gas turbine (SOFC–MGT) hybrid systems fueled by methanol and di-methyl-ether (DME). Energy 2009;34(12):2124–30. http://dx.doi.org/10.1016/j.energy.2008.09.013.
[13] Buonomano A, Calise F, d'Accadia MD, Palombo A, Vicidomini M. Hybrid solid oxide fuel cells–gas turbine systems for combined heat and power: A review. Appl Energy 2015;156:32–85. http://dx.doi.org/10.1016/j.apenergy.2015.06.027, Review SOFC-GT systems.
[14] Stiller C, Thorud B, Bolland O, Kandepu R, Imsland L. Control strategy for a solid oxide fuel cell and gas turbine hybrid system. J Power Sources 2006;158(1):303–15. http://dx.doi.org/10.1016/j.jpowsour.2005.09.010.
[15] Chuahy FDF, Kokjohn SL. Solid oxide fuel cell and advanced combustion engine combined cycle: A pathway to 70% electrical efficiency. Appl Energy 2019;235:391–408. http://dx.doi.org/10.1016/j.apenergy.2018.10.132.
[16] Sapra H, et al. Integration of solid oxide fuel cell and internal combustion engine for maritime applications. Appl Energy 2021;281. http://dx.doi.org/10.1016/j.apenergy.2020.115854.
[17] Oh D, Cho D, Kim T. Design and evaluation of hybrid propulsion ship powered by fuel cell and bottoming cycle. Int J Hydrog Energy 2023;48(22):8273–85. http://dx.doi.org/10.1016/j.ijhydene.2022.11.157.
[18] Rokni M. Thermodynamic analysis of an integrated solid oxide fuel cell cycle with a rankine cycle. Energy Convers Manage 2010;51(12):2724–32. http://dx.doi.org/10.1016/j.enconman.2010.06.008.
[19] Arsalis A. Thermoeconomic modeling and parametric study of hybrid SOFC–gas turbine–steam turbine power plants ranging from 1.5 to 10MWe. J Power Sources 2008;181(2):313–26. http://dx.doi.org/10.1016/j.jpowsour.2007.11.104.
[20] Yadav AK, Sinha S, Kumar A. Techno-economic and environmental analysis of hybrid SOFC-GT-sCO2 systems for sustainable energy generation. Int J Hydrog Energy 2025;120:558–71. http://dx.doi.org/10.1016/j.ijhydene.2025.03.238.
[21] Schöffer SI, Klein SA, Aravind PV, Pecnik R. A solid oxide fuel cell- supercritical carbon dioxide Brayton cycle hybrid system. Appl Energy 2021;283. http://dx.doi.org/10.1016/j.apenergy.2020.115748.
[22] Mojaver P, Abbasalizadeh M, Khalilarya S, Chitsaz A. Co-generation of electricity and heating using a SOFC-ScCO2 Brayton cycle-ORC integrated plant: Investigation and multi-objective optimization. Int J Hydrog Energy 2020;45(51):27713–29. http://dx.doi.org/10.1016/j.ijhydene.2020.07.137.
[23] He V, Gaffuri M, Van herle J, Schiffmann J. Readiness evaluation of SOFC-MGT hybrid systems with carbon capture for distributed combined heat and power. Energy Convers Manage 2023;278. http://dx.doi.org/10.1016/j.enconman.2023.116728.
[24] Azizi MA, Brouwer J. Progress in solid oxide fuel cell-gas turbine hybrid power systems: System design and analysis, transient operation, controls and optimization. Appl Energy 2018;215:237–89. http://dx.doi.org/10.1016/j.apenergy.2018.01.098.
[25] Peters R, Deja R, Blum L, Pennanen J, Kiviaho J, Hakala T. Analysis of solid oxide fuel cell system concepts with anode recycling. Int J Hydrog Energy 2013;38(16):6809–20. http://dx.doi.org/10.1016/j.ijhydene.2013.03.110.

[26] Braga LB, Silveira JL, Evaristo da Silva M, Machin EB, Pedroso DT, Tuna CE. Comparative analysis between a PEM fuel cell and an internal combustion engine driving an electricity generator: Technical, economical and ecological aspects. Appl Therm Eng 2014;63(1):354–61. http://dx.doi.org/10.1016/j.applthermaleng.2013.10.053.
[27] Nautilus. The comparison of different technologies for on-board power supply of cruise ships. Report, 2022.
[28] European Maritime Safety Agency. Potential of hydrogen as fuel for shipping. Report, EMSA; 2023.
[29] Kim HR, Seo MH, Ahn JH, Kim TS. Thermodynamic design and analysis of SOFC/PEMFC hybrid systems with cascade effects: A perspective on complete carbon dioxide capture and high efficiency. Energy Rep 2023;9:2335–47. http://dx.doi.org/10.1016/j.egyr.2023.01.048, Using the PEMFC for carbon capture downstream of SOFC.
[30] Wang F, et al. A comprehensive review on high-temperature fuel cells with carbon capture. Appl Energy 2020;275. http://dx.doi.org/10.1016/j.apenergy.2020.115342.
[31] Wu Z, Zhang Z, Ni M. Modeling of a novel SOFC-PEMFC hybrid system coupled with thermal swing adsorption for H2 purification: Parametric and exergy analyses. Energy Convers Manage 2018;174:802–13. http://dx.doi.org/10.1016/j.enconman.2018.08.073.
[32] Cai W, et al. Integrating a Pd-Ag membrane for hydrogen purification and recirculation in a direct ammonia fueled SOFC-PEMFC system. Int J Hydrog Energy 2024;95:570–82. http://dx.doi.org/10.1016/j.ijhydene.2024.11.220.
[33] Tan LJ, Yang C, Zhou N. Performance of the solid oxide fuel cell (SOFC)/proton-exchange membrane fuel cell (PEMFC) hybrid system. Chem Eng Technol 2016;39(4):689–98. http://dx.doi.org/10.1002/ceat.201500424.
[34] Meng T, Cui D, Ji Y, Cheng M, Tu B, Lan Z. Optimization and efficiency analysis of methanol SOFC-PEMFC hybrid system. Int J Hydrog Energy 2022;47(64):27690–702. http://dx.doi.org/10.1016/j.ijhydene.2022.06.102.
[35] Meng T, et al. Performance evaluation of high-efficiency SOFC-PEMFC hybrid system fueled by liquid ammonia. Int J Hydrog Energy 2023;48(79):30887–98. http://dx.doi.org/10.1016/j.ijhydene.2023.04.222.
[36] Rabbani A, Rokni M. Modeling and analysis of transport processes and efficiency of combined SOFC and PEMFC systems. Energies 2014;7(9):5502–22. http://dx.doi.org/10.3390/en7095502, Great parametric analysis on SOFC-PEMFC.
[37] Aravind PV, Woudstra T, Woudstra N, Spliethoff H. Thermodynamic evaluation of small-scale systems with biomass gasifiers, solid oxide fuel cells with Ni/GDC anodes and gas turbines. J Power Sources 2009;190(2):461–75. http://dx.doi.org/10.1016/j.jpowsour.2009.01.017.
[38] Woudstra N, van der Stelt TP, Hemmes K. The thermodynamic evaluation and optimization of fuel cell systems. J Fuel Cell Sci Technol 2006;3:155–64. http://dx.doi.org/10.1115/1.2174064.
[39] Liso V, Olesen AC, Nielsen MP, Kær SK. Performance comparison between partial oxidation and methane steam reforming processes for solid oxide fuel cell (SOFC) micro combined heat and power (CHP) system. Energy 2011;36(7):4216–26. http://dx.doi.org/10.1016/j.energy.2011.04.022.
[40] Aguiar P, Chadwick D, Kershenbaum L. Modelling of an indirect internal reforming solid oxide fuel cell. Chem Eng Sci 2002;57:1665–77.
[41] Wang R, et al. Control of carbon deposition over methane-fueled SOFCs through tuning the O/C ratio at the anode/electrolyte interface. J Power Sources 2022;544. http://dx.doi.org/10.1016/j.jpowsour.2022.231854.
[42] Riensche E, Stimming U, Unverzagt G. Optimization of a 200 kW SOFC cogeneration power plant. Part 1: Variation of process parameters. J Power Sources 1998;73:251–6.
[43] Riensche E, Meusinger J, Stimming U, Unverzagt G. Optimization of a 200 kW SOFC cogeneration power plant. Part 2: variation of the flowsheet. J Power Sources 1998;71:306–14.
[44] TeGrotenhuis WE, King DL, Brooks KP, Golladay BJ, Wegeng RS. Optimizing microchannel reactors by trading-off equilibrium and reaction kinetics through temperature management. In: International conference on microreaction technology.
[45] Valdés-López VF, Mason T, Shearing PR, Brett DJL. Carbon monoxide poisoning and mitigation strategies for polymer electrolyte membrane fuel cells – A review. Prog Energy Combust Sci 2020;79. http://dx.doi.org/10.1016/j.pecs.2020.100842.
[46] Ritter JA, Ebner AD. State-of-the-art adsorption and membrane separation processes for hydrogen production in the chemical and petrochemical industries. Sep Sci Technol 2007;42(6):1123–93. http://dx.doi.org/10.1080/01496390701242194, ISSN: 0149-6395 1520-5754.
[47] You YW, Lee DG, Yoon KY, Moon DK, Kim SM, Lee CH. H2 PSA purifier for CO removal from hydrogen mixtures. Int J Hydrog Energy 2012;37(23):18175–86. http://dx.doi.org/10.1016/j.ijhydene.2012.09.044.
[48] IVYS. Pressure Swing Adsorption - systems for ultra-pure hydrogen & other industry gas purification [Brochure]. Catalog. URL: ivysads.com/product/h3200-series-hydrogen-purifier/.
[49] Nedstack fuel cell technology bv. Nedstack FCS 10-XXL PEM fuel cell stack. 2019, Catalog. URL: https://nedstack.com/sites/default/files/2019-11/20191105_nedstack_fcs_10-xxl.pdf.
[50] de Groot A. Advanced exergy analysis of high temperature fuel cell systems (Thesis), 2004.
[51] Hemmes K, Patil A, Woudstra N. Internal reforming SOFC system for flexible coproduction of hydrogen and power. In: Conference paper. 2005, p. 577–82. http://dx.doi.org/10.1115/fuelcell2005-74153.
[52] Doosan Fuel Cell. SOFC S300 NG. 2025, Web Page. URL: www.doosanfuelcell.com/en/prod/prod-0201/.
[53] Bloom Energy. The bloom energy server 6.5. Catalog, 2024.
[54] SolydEra. SolydEra Power Module PM-X [Brochure]. Catalog.
[55] NedStack. Modular fuel cell power solutions [Brochure]. Catalog.
[56] Ballard. FCwave - Fuel cell power module for marine applications [Brochure]. Catalog, 2024.
[57] PowerCell. Marine system 225 [Brochure]. Catalog, 2025.
[58] Engelbracht M, Peters R, Blum L, Stolten D. Analysis of a solid oxide fuel cell system with low temperature anode off-gas recirculation. J Electrochem Soc 2015;162(9):F982–7. http://dx.doi.org/10.1149/2.0371509jes.
[59] van Biert L, Visser K, Aravind PV. A comparison of steam reforming concepts in solid oxide fuel cell systems. Appl Energy 2020;264. http://dx.doi.org/10.1016/j.apenergy.2020.114748.
[60] Tarroja B, Mueller F, Maclay J, Brouwer J. Parametric thermodynamic analysis of a solid oxide fuel cell gas turbine system design space. J Eng Gas Turbines Power 2010;132. http://dx.doi.org/10.1115/1.4000263.
[61] Nehter P. A high fuel utilizing solid oxide fuel cell cycle with regard to the formation of nickel oxide and power density. J Power Sources 2007;164(1):252–9. http://dx.doi.org/10.1016/j.jpowsour.2006.08.037.